



Cite this: *Nanoscale*, 2022, **14**, 12620

# Feasibility of switchable dual function materials as a flexible technology for CO<sub>2</sub> capture and utilisation and evidence of passive direct air capture†

Loukia-Pantzechroula Merkouri,<sup>a</sup> Tomas Ramirez Reina  <sup>\*a,b</sup> and  
Melis S. Duyar  <sup>\*a</sup>

The feasibility of a Dual Function Material (DFM) with a versatile catalyst offering switchable chemical synthesis from carbon dioxide (CO<sub>2</sub>) was demonstrated for the first time, showing evidence of the ability of these DFMs to passively capture CO<sub>2</sub> directly from the air as well. These DFMs open up possibilities in flexible chemical production from dilute sources of CO<sub>2</sub>, through a combination of CO<sub>2</sub> adsorption and subsequent chemical transformation (methanation, reverse water gas shift or dry reforming of methane). Combinations of Ni Ru bimetallic catalyst with Na<sub>2</sub>O, K<sub>2</sub>O or CaO adsorbent were supported on CeO<sub>2</sub>–Al<sub>2</sub>O<sub>3</sub> to develop flexible DFMs. The designed multicomponent materials were shown to reversibly adsorb CO<sub>2</sub> between the 350 and 650 °C temperature range and were easily regenerated by an inert gas purge stream. The components of the flexible DFMs showed a high degree of interaction with each other, which evidently enhanced their CO<sub>2</sub> capture performance ranging from 0.14 to 0.49 mol kg<sup>−1</sup>. It was shown that captured CO<sub>2</sub> could be converted into useful products through either CO<sub>2</sub> methanation, reverse water–gas shift (RWGS) or dry reforming of methane (DRM), which provides flexibility in terms of co-reactant (hydrogen vs. methane) and end product (synthetic natural gas, syngas or CO) by adjusting reaction conditions. The best DFM was the one containing CaO, producing 104 μmol of CH<sub>4</sub> per kg<sub>DFM</sub> in CO<sub>2</sub> methanation, 58 μmol of CO per kg<sub>DFM</sub> in RWGS and 338 μmol of CO per kg<sub>DFM</sub> in DRM.

Received 15th May 2022,  
Accepted 11th August 2022  
DOI: 10.1039/d2nr02688k

rsc.li/nanoscale

## 1. Introduction

Global warming is increasing at an alarming rate, as carbon dioxide (CO<sub>2</sub>) emissions reached 33 Gt in 2021.<sup>1</sup> Efforts, such as the Paris Agreement in 2015, are continuously made in attempt to control greenhouse gas concentrations and thus the extent of global warming,<sup>2</sup> while there is a need to achieve net zero CO<sub>2</sub> emissions by 2050 and have a substantial decrease in CO<sub>2</sub> emissions after 2030.<sup>3</sup> A solution to control CO<sub>2</sub> emissions is Carbon Capture, Utilisation and Storage (CCUS).<sup>4</sup> The current state-of-the-art technologies in terms of CO<sub>2</sub> capture include the widely commercialised amine absorption systems.<sup>5–8</sup> An alternative to amine absorption is solid adsorption, *e.g.* metal organic frameworks MOFs, zeolites, and alkali/alkaline oxides/carbonates. During adsorption, CO<sub>2</sub> is either chemisorbed or physisorbed onto the adsorbent's surface until

breakthrough, or saturation, is reached. The desorption of a concentrated CO<sub>2</sub> stream usually occurs *via* a pressure or temperature swing process.<sup>5,9</sup> The CO<sub>2</sub> utilisation step involves the use of CO<sub>2</sub> to produce added-value chemicals and fuels and is appealing because of the need for carbon in the chemical industry to produce chemicals. Currently CO<sub>2</sub> is used mainly in the production of urea (~160 Mt per year). However, CO<sub>2</sub> being a highly stable molecule thermodynamically, catalysts are needed for its conversion into various products.<sup>8,10–12</sup>

As far as the CO<sub>2</sub> catalytic upgrading routes are concerned, the dry reforming of methane (DRM),<sup>13–15</sup> the reverse water–gas shift (RWGS)<sup>16–19</sup> and the CO<sub>2</sub> methanation reactions<sup>16,20,21</sup> have attracted substantial attention in recent years. In DRM (eqn (1)), two of the most harmful greenhouse gases (CO<sub>2</sub> and CH<sub>4</sub>) react to form syngas, which is a mixture of carbon monoxide (CO) and hydrogen (H<sub>2</sub>). DRM can be used for biogas upgrading purposes because biogas is mainly a mixture of CO<sub>2</sub> and methane (CH<sub>4</sub>). DRM requires high temperatures and catalysts developed for DRM are susceptible to deactivation *via* coke formation.<sup>8,13</sup> In RWGS (eqn (2)), hydrogen is used to reduce CO<sub>2</sub> to CO while producing water as byproduct. CO is an important chemical reagent for industrial chemicals synthesis such as through carbonylation reac-

<sup>a</sup>Department of Chemical and Process Engineering, University of Surrey, Guildford, GU2 7XH UK. E-mail: m.duyar@surrey.ac.uk, t.ramirezreina@surrey.ac.uk

<sup>b</sup>Department of Inorganic Chemistry and Materials Sciences Institute, University of Seville-CSIC, 41092 Seville, Spain

† Electronic supplementary information (ESI) available. See DOI: <https://doi.org/10.1039/d2nr02688k>



tions. Careful catalyst design is necessary, to ensure selectivity towards CO and to overcome the competition with the CO<sub>2</sub> methanation reaction. H<sub>2</sub>/CO ratio can be adjusted *via* the RWGS reaction to increase conversion while yielding a specific mixture of CO and H<sub>2</sub> (known as syngas) that can then be used for downstream chemicals production *via* methanol synthesis or Fischer–Tropsch synthesis.<sup>8,10,16,22</sup> CO<sub>2</sub> methanation (eqn (3)), which is another CO<sub>2</sub> hydrogenation reaction, can be used for the production of CH<sub>4</sub>, or synthetic natural gas. This reaction attracted a lot of attention both in the 1970s, during the oil crisis, and nowadays, because of its possible use in power to gas schemes. As CO<sub>2</sub> methanation is favoured at lower temperatures, active catalysts are needed for overcoming significant kinetic limitations.<sup>8,10,23</sup> The aforementioned reactions are presented below.

DRM:



RWGS:



CO<sub>2</sub> methanation:



The use of Dual Function Materials (DFMs) integrates CO<sub>2</sub> capture and utilisation to lower the energy demands, and thus the cost of CCU processes through a process intensification approach.<sup>24</sup> They are designed to work in cyclic operation, *i.e.* in successive CO<sub>2</sub> capture and reduction cycles based on a spill over mechanism.<sup>25–27</sup> DFMs are able to capture the CO<sub>2</sub> from a flue gas stream or air and then to catalyse it to produce various chemicals based on the co-reactant used. The most studied catalytic materials are the noble metals, like ruthenium (Ru) and rhodium (Rh) due to their increased catalytic activity in the DRM, RWGS and CO<sub>2</sub> methanation reactions. However, their high cost can be prohibitive and efforts are made to use cheaper, but highly active materials, such as nickel (Ni). The most studied reaction for the DFMs application to date is CO<sub>2</sub> methanation.<sup>28–31</sup> This reaction offers an isothermal solution to the DFMs system because the exothermicity of the CO<sub>2</sub> methanation can supply the required heat for the CO<sub>2</sub> desorption and its spill-over onto the catalytic sites.<sup>24,27,32</sup> The development of DFMs in the RWGS and DRM is still in its infancy, but several studies in RWGS<sup>33–37</sup> and DRM<sup>38–41</sup> have shown potential and are worthy of notice because the DFMs overcome their current limitations. A comprehensive summary of all DFMs studied can be found in some recent reviews.<sup>28–31,42</sup>

In our previous study, we examined the feasibility of using a switchable catalyst to catalyse the CO<sub>2</sub> methanation, RWGS, and DRM reactions that offers flexibility in terms of CO<sub>2</sub> utilisation in a changing energy landscape,<sup>43</sup> while other studies exist in literature.<sup>44,45</sup> It was shown that a combination of Ni and Ru onto a ceria oxide–alumina oxide support (CeO<sub>2</sub>–Al<sub>2</sub>O<sub>3</sub>) was able to efficiently catalyse all three reactions

(“switching” between them) by simply changing the reaction conditions, *i.e.* the co-reactant and the temperature. Herein, we present the flexible DFMs, which combine one of three adsorbents (Na<sub>2</sub>O, K<sub>2</sub>O or CaO) with the Ni–Ru switchable catalyst. This study is the proof of concept for switchable DFMs. CeO<sub>2</sub> was used as a support in combination with the widely used in DFMs Al<sub>2</sub>O<sub>3</sub> due to its excellent redox properties and its important role in the CO<sub>2</sub> adsorption and conversion to various products.<sup>43,44,46,47</sup> The addition of Ru to Ni was chosen due to its ease of transformation between its oxides and metallic species which is carried out at low temperatures and is helpful when CO<sub>2</sub> capture is performed in a realistic oxidising environment. Their combination has also been effective to enable product versatility since their strong interaction leads to electronically rich surfaces which are active sites for reactants activation.<sup>43,44</sup>

The switchable DFMs system integrates the benefits of DFMs, as described earlier, with switchable catalysts. The flexibility in chemical synthesis offers a solution to the changing energy sector in the near-term future and resilience against the fluctuation in the supply and demand of chemicals. It is known that there is a seasonal and annual demand change; for example, methane is currently used for residential heating in the winter, but hydrogen is considered for use as residential fuel in the future.<sup>48</sup> Flexible DFMs allow versatile process designs that can work in different modes. For instance, synthetic natural gas may be produced when excess renewable electricity exists or when more heating is needed during winter, while by simply changing the reactor conditions, syngas or CO may be produced to act as a building block in the chemical industry for the production of dimethyl ether, urea, methanol and hydrocarbons. Herein we demonstrate the feasibility of switchable DFMs for the first time, while exploring the adsorption of CO<sub>2</sub> at different temperatures and evaluating the design principles needed to develop DFMs for switchable operation.

## 2. Experimental

### 2.1. Dual function materials synthesis

The three DFMs of this study were prepared by sequential impregnation. The adsorbents were impregnated onto the CeO<sub>2</sub>–Al<sub>2</sub>O<sub>3</sub> support and then, the two transition metals, Ni and Ru, were impregnated onto the supported adsorbents, as it was previously shown that impregnating metals on adsorbents resulted in better DFMs performance.<sup>24</sup> Table 1 shows the designed materials composition and the abbreviations used in this work.

Supported adsorbents were prepared by initially mixing the required amounts of the CeO<sub>2</sub>–Al<sub>2</sub>O<sub>3</sub> support (SCFa-160 Ce20 Puralox, Sasol) and NaNO<sub>3</sub> (Fluka), KNO<sub>3</sub> (Sigma Aldrich), and Ca(NO<sub>3</sub>)<sub>2</sub>·4H<sub>2</sub>O (Sigma Aldrich) with deionised water. The suspensions were then mixed at room temperature with a magnetic stirrer and the excess water was removed in a rotary evaporator under reduced pressure. Afterwards, they were dried



Table 1 Materials composition and abbreviations

Material	Abbreviation	Catalyst loading (wt%)	Adsorbent loading (wt%)
Na <sub>2</sub> O/CeO <sub>2</sub> -Al <sub>2</sub> O <sub>3</sub>	Na	—	11.9 wt% Na <sub>2</sub> O
K <sub>2</sub> O/CeO <sub>2</sub> -Al <sub>2</sub> O <sub>3</sub>	K	—	11.9 wt% K <sub>2</sub> O
CaO/CeO <sub>2</sub> -Al <sub>2</sub> O <sub>3</sub>	Ca	—	11.9 wt% CaO
Ni-Ru/CeO <sub>2</sub> -Al <sub>2</sub> O <sub>3</sub>	NiRu	15 wt% Ni, 1 wt% Ru	—
Ni-Ru, Na <sub>2</sub> O/CeO <sub>2</sub> -Al <sub>2</sub> O <sub>3</sub>	NiRuNa	15 wt% Ni, 1 wt% Ru	10 wt% Na <sub>2</sub> O
Ni-Ru, K <sub>2</sub> O/CeO <sub>2</sub> -Al <sub>2</sub> O <sub>3</sub>	NiRuK	15 wt% Ni, 1 wt% Ru	10 wt% K <sub>2</sub> O
Ni-Ru, CaO/CeO <sub>2</sub> -Al <sub>2</sub> O <sub>3</sub>	NiRuCa	15 wt% Ni, 1 wt% Ru	10 wt% CaO

overnight at 120 °C and calcined at 400 °C for 4 hours (5 °C min<sup>-1</sup>). The resulting supported adsorbents were the Na<sub>2</sub>O/CeO<sub>2</sub>-Al<sub>2</sub>O<sub>3</sub>, K<sub>2</sub>O/CeO<sub>2</sub>-Al<sub>2</sub>O<sub>3</sub>, and CaO/CeO<sub>2</sub>-Al<sub>2</sub>O<sub>3</sub>.

A similar impregnation procedure was performed when synthesising the three DFMs. The required amounts of Ni(NO<sub>3</sub>)<sub>2</sub>·6H<sub>2</sub>O (Acros Organics) and Ru(NO)(NO<sub>3</sub>)<sub>3</sub> solution (1.5 w/v Ru, Alfa Aesar) were mixed with the supported adsorbents in order to obtain 15 wt% Ni and 1 wt% Ru. These were mixed with excess deionised water, which was then removed in a rotary evaporator under reduced pressure, dried overnight at 120 °C, and calcined at 500 °C for 3 hours (5 °C min<sup>-1</sup>). The amount of adsorbent precursor used for the supported adsorbents was adjusted to give a final DFMs loading of 10 wt% of the respective oxides and so the resulting supported adsorbents had 11.9 wt% Na<sub>2</sub>O, K<sub>2</sub>O, and CaO. Therefore, the prepared DFMs were the 15 wt% Ni, 1 wt% Ru-10 wt% Na<sub>2</sub>O/CeO<sub>2</sub>-Al<sub>2</sub>O<sub>3</sub>, the 15 wt% Ni, 1 wt% Ru-10 wt% K<sub>2</sub>O/CeO<sub>2</sub>-Al<sub>2</sub>O<sub>3</sub>, and the 15 wt% Ni, 1 wt% Ru-10 wt% CaO/CeO<sub>2</sub>-Al<sub>2</sub>O<sub>3</sub>. In some experiments, the 15 wt% Ni, 1 wt% Ru/CeO<sub>2</sub>-Al<sub>2</sub>O<sub>3</sub> switchable catalyst, whose synthesis method was described in,<sup>43</sup> was used as a reference material so as to show the impact of the addition of the adsorbents. In order for the supported adsorbents to have the same heat treatment as DFMs, they were recalined at 500 °C for 3 hours (5 °C min<sup>-1</sup>). For the sake of simplicity, the supported adsorbents were called Na, K, and Ca, the DFMs, NiRuNa, NiRuK, and NiRuCa, and the switchable catalyst NiRu.

## 2.2. Characterisation

The Brunauer-Emmett-Teller (BET) equation and the Barrett-Joyner-Halenda (BJH) methods were used to obtain the specific surface area and pore volume of the materials. Initially, degassing at 250 °C in vacuum for 4 hours took place and then, the textural properties of the materials were determined by nitrogen adsorption-desorption measurements at -195 °C in a Micrometrics 3Flex apparatus.

X-ray Diffraction (XRD) was performed on fresh supported adsorbents and on fresh, reduced, and spent DFMs in a X'Pert Powder from PANalytical apparatus. The diffraction patterns were obtained at 30 mA and 40 kV by using Cu K $\alpha$  radiation ( $\lambda$  = 0.154 nm). The 2 $\theta$  angle was increased every 450 seconds by 0.05° in the range of 10–90°.

Scanning Electron Microscopy (SEM) was carried out on the fresh supported adsorbents and DFMs by using a JEOL JSM-7100F instrument, which also had an Energy Dispersive

X-ray Spectroscopy (EDS) analyser. Carbon paint was used to fix the samples to the holder and gold coating was conducted to eliminate the charging effects.

Transmission Electron Microscopy (TEM) was carried out on the reduced DFMs in a Talos F200I instrument from ThermoFisher with an electron source of 200 kV. The DFMs were reduced *ex situ* at 800 °C for 1 hour at a 50 ml min<sup>-1</sup> total flow rate of a 10% H<sub>2</sub>/N<sub>2</sub> mixture. To prepare the TEM samples, the materials were dispersed in ethanol in an ultrasonic bath, dropped onto copper grids coated with lacey carbon film and dried. Prior to sample insertion in the instrument, the specimen holder with the sample was dried in a UV furnace.

H<sub>2</sub>-Temperature Programmed Reduction (H<sub>2</sub>-TPR) was performed on the fresh (after calcination) DFMs in fixed bed quartz reactor. The data were logged by using the Quadra software package and the H<sub>2</sub> consumption was observed in an online mass spectrometer (Omni-Star GSD 320). A 10% H<sub>2</sub>/Ar mixture with a total flow of 50 ml min<sup>-1</sup> was passed through the reactor with 50 mg of sample while the temperature was raised from room temperature to 950 °C with 10 °C min<sup>-1</sup> rate.

CH<sub>4</sub>-Temperature Programmed Surface Reaction (CH<sub>4</sub>-TSPR) was conducted on the fresh NiRuCa sample in a fixed bed reactor similar to H<sub>2</sub>-TPR experiments. In this experiment, 30 mg of fresh (after calcination) NiRuCa was used and the temperature was increased from room temperature to 950 °C (10 °C min<sup>-1</sup>) with a pure CH<sub>4</sub> feed of 30 ml min<sup>-1</sup>. No N<sub>2</sub> was used in the feed in order the mass to charge ratio (*m/z*) of 28 to be solely attributed to CO.

CO<sub>2</sub>-Temperature Programmed Desorption (CO<sub>2</sub>-TPD) was carried out on fresh DFMs and adsorbents in a fixed bed quartz reactor. In the CO<sub>2</sub>-TPD experiments, 50 mg of sample were initially reduced *in situ* at 800 °C for 1 hour with a 10% H<sub>2</sub>/N<sub>2</sub> mixture and a total flow of 50 ml min<sup>-1</sup> (10 °C min<sup>-1</sup>). After cooling down to 40 °C with a N<sub>2</sub> purge, a 50 ml min<sup>-1</sup> flow of a 10% CO<sub>2</sub>/N<sub>2</sub> mixture was used for 45 minutes to saturate the samples. Subsequently, 50 ml min<sup>-1</sup> of N<sub>2</sub> was introduced through the reactor to remove the weakly adsorbed CO<sub>2</sub> for 30 minutes and, finally, the temperature was raised to 800 °C at a 10 °C min<sup>-1</sup> rate. The mass to charge ratio (*m/z*) of 44 corresponding to CO<sub>2</sub> was recorded using an online mass spectrometer (Omni-Star GSD 320) during the temperature ramp.

Thermogravimetric Analysis (TGA) was performed on the reduced and post-reaction DFMs in an SDT650 apparatus from



TA Instruments in order to measure the amount of carbon depositions. A flow of  $100 \text{ mL min}^{-1}$  of air was employed while the temperature was raised from room temperature to  $950^\circ\text{C}$  at a  $10^\circ\text{C min}^{-1}$  rate.

### 2.3. Performance testing

**2.3.1. Adsorption and desorption study at different temperatures.** An SDT650 apparatus from TA Instruments was used so as to understand the adsorption and desorption behaviour of the materials at different temperatures. 10–15 mg of a reduced sample was used in each run. Firstly, the temperature was increased from room temperature to  $150^\circ\text{C}$  with  $100 \text{ mL min}^{-1}$  of Ar at a  $10^\circ\text{C min}^{-1}$  rate and was held at that temperature for 30 minutes in order for all the weakly adsorbed gases to be desorbed. Next, it was raised to  $350^\circ\text{C}$ ,  $450^\circ\text{C}$ ,  $550^\circ\text{C}$ , or  $650^\circ\text{C}$  with the same Ar flow and temperature rate as before. Subsequently, the temperature was stabilised at the desired level for 200 minutes, allowing 5 cycles to be conducted, each of which consisted of 20 minutes of  $\text{CO}_2$  adsorption and 20 minutes of  $\text{CO}_2$  desorption. In each adsorption step,  $20 \text{ mL min}^{-1}$  of  $\text{CO}_2$  and  $100 \text{ mL min}^{-1}$  of Ar were used and in each desorption step,  $100 \text{ mL min}^{-1}$  of Ar. The test was carried out on the reduced supported adsorbents, switchable catalyst and DFMs. The reduction was performed *ex situ* at  $800^\circ\text{C}$  for 1 hour at a  $50 \text{ mL min}^{-1}$  total flow rate of a 10%  $\text{H}_2/\text{N}_2$  mixture.

**2.3.2. Feasibility study of flexible DFMs.** The three DFMs were tested in a tubular fixed bed quartz reactor (0.5 in OD) at atmospheric pressure and were supported on a quartz wool bed. The volumetric percentages of  $\text{CO}_2$ ,  $\text{CH}_4$ , CO, and  $\text{H}_2$  in the outlet stream were monitored, using an ABB AO2020 online gas analyser, which was placed after the water was condensed and separated in a chiller. In the ABB AO2020 online gas analyser, infrared gas detectors were used for  $\text{CO}_2$ ,  $\text{CH}_4$  and CO and thermal conductivity for  $\text{H}_2$ . A bubble meter was used to allow the accurate measurement of the total volumetric flow rate. Two different modes of experimental set up were used in those feasibility experiments: the 'reactor' mode and the 'bypass' mode. In the former, the desired gases were passing through the reactor, whereas in the latter, they were bypassing it, going to the condenser and then to the ABB gas analyser or the bubble meter. A simplified process diagram is shown in Fig. 1 below.

Each DFM was tested for methanation, RWGS and DRM applications in that order. Initially, 250 mg of sample were reduced *in situ* at  $800^\circ\text{C}$  for 1 hour at a  $50 \text{ mL min}^{-1}$  total flow rate of a 10%  $\text{H}_2/\text{N}_2$  mixture ( $10^\circ\text{C min}^{-1}$ ). Then, the temperature was decreased to  $350^\circ\text{C}$  with a  $\text{N}_2$  purge stream in order to perform a cycle of  $\text{CO}_2$  capture- $\text{N}_2$  purge- $\text{CO}_2$  methanation. The  $\text{CO}_2$  capture step was performed in the 'reactor' mode with a 10%  $\text{CO}_2/\text{N}_2$  mixture of  $50 \text{ mL min}^{-1}$  total flow rate for 20 minutes. After the 20 minutes had elapsed, a 10 minute  $\text{N}_2$  purge step was carried out, resulting in the removal of the weakly adsorbed  $\text{CO}_2$  and ensuring no cross-mixing of  $\text{CO}_2$  and  $\text{H}_2$ . This purge step was continued until a zero  $\text{CO}_2$  reading in the gas analyser was obtained so as to demonstrate

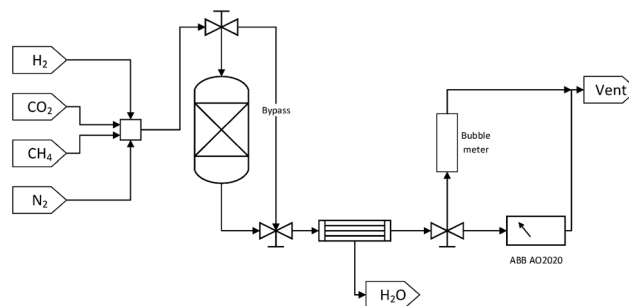


Fig. 1 Simplified process flow diagram for experimental set up.

that the produced gases were formed from the captured  $\text{CO}_2$ . Subsequently, in the 'bypass' mode, a mixture containing 10% of  $\text{H}_2$  in  $\text{N}_2$  was introduced through the system until its reading in the analyser was stabilised and then the stream was switched to pass through the reactor. This constituted the reaction step which was performed for 20 minutes. Once the  $\text{CO}_2$  capture- $\text{N}_2$  purge- $\text{CO}_2$  methanation cycle was carried out at  $350^\circ\text{C}$ , the temperature was increased to  $650^\circ\text{C}$  at a  $10^\circ\text{C min}^{-1}$  rate. A cycle of  $\text{CO}_2$  capture- $\text{N}_2$  purge-RWGS and a cycle of  $\text{CO}_2$  capture- $\text{N}_2$  purge-DRM followed as described above, but in the case of DRM,  $\text{CH}_4$  instead of  $\text{H}_2$  was used as co-reactant. A  $\text{N}_2$  purge step was also used following the  $\text{CO}_2$  methanation reaction and prior to the heating-up step for 10 minutes, as well as after the RWGS reaction and before the  $\text{CO}_2$  capture step in order to obtain zero readings in the gas analyser.

It is worth noting that the  $\text{N}_2$  flow remained the same throughout the experiment as in all the  $\text{CO}_2$  capture and reaction steps, making up 90% of the feed mixture in every case. The exact flow rate of  $\text{N}_2$  (*i.e.*  $45 \text{ mL min}^{-1}$ ) was measured at the beginning of the experiment so that it could be used as internal standard. This meant that when the total flow rates in  $\text{CO}_2$  capture and reaction steps were measured with the bubble meter, the exact flow rates of  $\text{CO}_2$  and co-reactant, either  $\text{H}_2$  or  $\text{CH}_4$ , were calculated by subtracting the known  $\text{N}_2$  flow rate from the corresponding total flow rate. Moreover, all the total volumetric flow rate measurements and the stabilisation of the gases percentage were performed in the 'bypass' mode to make sure that the DFMs were exposed to the desired gases only during the  $\text{CO}_2$  capture,  $\text{N}_2$  purge, and reaction steps.

In addition, the percentages of  $\text{CO}_2$ ,  $\text{CH}_4$ , CO, and  $\text{H}_2$  in the outlet stream shown in the gas analyser were recorded every 5 seconds throughout the experiment and it was assumed that the remaining volume percentage in the mixture was  $\text{N}_2$ . Hence, the volumetric flow rates of all gases were calculated according to the following formula, where the brackets represent the volumetric percentage of each gas, *i.e.*  $\text{CO}_2$ ,  $\text{CH}_4$ , CO, and  $\text{H}_2$ , the  $F$  the flow rate ( $\text{mL min}^{-1}$ ), and the subscript 'i' the respective gas. The amount of products (in mL) was calculated based on the area under the curve at a flow rate ( $\text{mL min}^{-1}$ ) vs. time (min) graph.

$$F_i = \frac{[i]}{[\text{N}_2]} \times F_{\text{N}_2} \quad (4)$$





### 3. Results and discussion

#### 3.1. Performance testing

**3.1.1. Adsorption and desorption studies in TGA.** Switchable DFMs need to be able to operate in the 350–650 °C temperature range to be able to perform all of the RWGS, methanation and DRM reactions, which makes it essential to promote adsorption of CO<sub>2</sub> in this temperature range. CO<sub>2</sub> adsorption is an exothermic process and it is favoured at lower temperatures, which can make a lot of different (low and intermediate temperature) adsorbents suitable for DFMs performing only CO<sub>2</sub> methanation, a reaction that is thermodynamically favoured at lower temperatures.<sup>28</sup> To evaluate cyclic CO<sub>2</sub> adsorption capacity of adsorbent and DFMs developed in this work, 5 cycles of CO<sub>2</sub> adsorption and desorption were performed at different temperatures. The results pertaining to the CO<sub>2</sub> adsorption and desorption performance of the DFMs are presented in Fig. 2 and S1,<sup>†</sup> those of the supported adsorbents in Fig. 3 and S2,<sup>†</sup> and the results from the reference NiRu catalyst are shown in Fig. S4.<sup>†</sup> Table 2 summarises the adsorption capacities of the DFMs at different temperatures based on their first cycle, while it includes CO<sub>2</sub> adsorption capacity information of similar DFM materials found in literature that show comparable results.

Fig. 1 shows that the DFMs designed in this study were able to reversibly adsorb CO<sub>2</sub> in the temperature range of 350–650 °C, making them suitable for the flexible DFMs scenario. They all displayed relatively high adsorption capacities without the requirement of high regeneration temperatures as the desorption was carried out by an inert gas purge. Concerning the NiRuNa sample, a drop in the adsorption

capacity was demonstrated with rising temperature, except when the temperature reached 650 °C. A similar trend was also observed in the NiRuCa sample. A pattern was not easily detected in the NiRuK sample, but it was noted that it had the best performance at intermediate temperatures, in accordance with the CO<sub>2</sub>-TPD results presented later. As a general outcome of this study, NiRuNa seemed to perform best at low temperatures, NiRuK at intermediate temperatures, and NiRuCa at high temperatures, in agreement with other findings<sup>49,50</sup> and following the logics of Pearson's hard/soft acid–base interactions. Nevertheless, these results indicated that it would be possible to use all of these materials as flexible DFMs at this temperature range. Indeed, the fact that the working adsorption capacity at 650 °C was even better than that of the DFMs at 350 °C was unexpected. However, it can be explained by a change in mechanism of CO<sub>2</sub> capture or a kinetic limitation, which had been overcome at 650 °C, as steeper slopes at higher temperatures are observed in Fig. S1.<sup>†</sup>

As can be seen in Fig. 1, a substantial amount of CO<sub>2</sub> was adsorbed during the first cycle for all DFMs, which was not the case in the supported adsorbents or the switchable catalyst. Especially at 350 °C, the adsorption capacity of the DFMs was higher than the supported adsorbents and the catalyst together, indicative of a synergy between those materials took place, which enhanced the CO<sub>2</sub> adsorption capacity. In other words, CO<sub>2</sub> was not adsorbed only onto the adsorbents and the catalysts, a fact that has already been established in literature.<sup>51,52</sup> Consequently, these results indicate that when adsorbents and catalysts are in close proximity, they benefit from each other, especially at high temperatures that the mechanism is kinetically activated. In fact, previous



Fig. 2 CO<sub>2</sub> Adsorption/desorption cycles of NiRuNa, NiRuK and NiRuCa at (A) 350 °C, (B) 450 °C, (C) 550 °C and (D) 650 °C.





Fig. 3 CO<sub>2</sub> Adsorption/desorption cycles of Na, K and Ca at (A) 350 °C and (B) 650 °C.

**Table 2** Summary of adsorption capacities of DFMs at different temperatures and comparison of similar DFMs from literature

DFM	Adsorption temperature (°C)	Adsorption capacity (mmol g <sub>DFM</sub> <sup>-1</sup> )	Ref.
15% Ni–1% Ru, 10% Na <sub>2</sub> O/CeO <sub>2</sub> –Al <sub>2</sub> O <sub>3</sub>	350	0.49	This work
	450	0.32	
	550	0.14	
	650	0.16	
15% Ni–1% Ru, 10% K <sub>2</sub> O/CeO <sub>2</sub> –Al <sub>2</sub> O <sub>3</sub>	350	0.29	This work
	450	0.17	
	550	0.15	
	650	0.18	
15% Ni–1% Ru, 10% CaO/CeO <sub>2</sub> –Al <sub>2</sub> O <sub>3</sub>	350	0.39	This work
	450	0.17	
	550	0.20	
	650	0.26	
1% Ru–10% Ni, 10% Na <sub>2</sub> CO <sub>3</sub> /Al <sub>2</sub> O <sub>3</sub>	350	0.27	56
	550	0.18	
1% Ce–10% Ni, 10% Na <sub>2</sub> CO <sub>3</sub> /Al <sub>2</sub> O <sub>3</sub>	350	0.16	56
	550	0.18	
1% Ru–10% Ni, 6.1% “Na <sub>2</sub> O”/Al <sub>2</sub> O <sub>3</sub>	320	0.52	25
10% Ni, 6.1% “Na <sub>2</sub> O”/Al <sub>2</sub> O <sub>3</sub>	320	0.40	25
5% Ru, 10% CaO/Al <sub>2</sub> O <sub>3</sub>	320	0.60	24
5% Ru, 10% Na <sub>2</sub> CO <sub>3</sub> /Al <sub>2</sub> O <sub>3</sub>	320	0.55	27
5% Ru, 6.1% “Na <sub>2</sub> O”/CeO <sub>2</sub>	320	0.37	57
5% Ru, 7.01% “K <sub>2</sub> O”/Al <sub>2</sub> O <sub>3</sub>	320	0.49	57

studies<sup>25,52</sup> demonstrated that both Ni and Ru were adsorbing CO<sub>2</sub> when combined in a DFM, which meant that spill over and methanation took place over onto both Ni and Ru sites. The findings showcase the importance of having one material performing both the CO<sub>2</sub> adsorption and reduction, rather than two different materials being mixed together. There can also be a role of CeO<sub>2</sub> in CO<sub>2</sub> adsorption because CeO<sub>2</sub> is known to promote CO<sub>2</sub> adsorption. After all, ceria is well known for its excellent redox properties<sup>35,46,53,54</sup> and further mechanistic studies need to be done in the future. Nevertheless, it was believed that a small quantity of CO<sub>2</sub> was used to oxidise the reduced ceria species and form CO.

Fig. S1–S3† show the amount of CO<sub>2</sub> adsorbed per mg of sample during those five cycles at different temperatures. All the materials demonstrated that the adsorption was performed in two steps. An initial fast adsorption of CO<sub>2</sub> took place,

accounting for the substantial weight gain at the beginning of each capture cycle. The second step was a slower one, evident from the change in slope. In addition, it was observed that the supported adsorbents were able to reach equilibrium and reversibly adsorb CO<sub>2</sub> onto the adsorbents' sites, meaning that they had managed to adsorb and desorb the same CO<sub>2</sub> amounts, which was not the case with the DFMs. An interesting observation was that there were different slopes for the “slow CO<sub>2</sub> adsorption step” in all DFMs when comparing the uptake behaviour at 650 °C to that at 350 °C, pointing to a kinetically limited capture mechanism that becomes favourable at higher temperatures. The different CO<sub>2</sub> adsorption mechanism at 350 °C and 650 °C could not be fully attributed to the former being weak chemisorption and the latter Ca, Na, K carbonate formation, because our TGA results shown in Fig. S2† demonstrated that the supported adsorbents reversibly adsorbed CO<sub>2</sub> at these temperatures. Hence, the formation of stable Ca, Na, K carbonates was not the main mechanism at this high temperature. Additionally, based on the CO<sub>2</sub>-TPD results shown below, these DFMs had a negligible amount of strong basic sites that could have favoured the carbonate formation. Therefore, it was found that the change in slope was not attributed to the adsorbents, but to the Ni–Ru species, as can be seen by comparing Fig. S1–S3† at 650 °C. This result also showcased that the catalytic component of the DFMs contributed to the CO<sub>2</sub> adsorption too, since various carbonate species have been reported for Ni–Ce catalysts in literature,<sup>55</sup> and highlighted the importance of a synergy between these two components. Nevertheless, a DRIFTS study is under way to identify the species responsible for this behaviour and for clarifying the differences in adsorption mechanisms.

**3.1.2. Feasibility study of flexible DFMs.** All DFMs were tested to evaluate their feasibility for use in a switchable operation scenario, by performing CO<sub>2</sub> capture and methanation first, followed by CO<sub>2</sub> capture and RWGS, then CO<sub>2</sub> capture and DRM. While this is not necessarily how these materials would operate (they might be used for DRM until a larger supply of green hydrogen becomes available, for instance), this testing methodology was chosen to facilitate comparison to our previous studies on switchable catalysts.<sup>43–45</sup> It is worth mentioning that the high reduction temperature was chosen due to RWGS and DRM being performed at high temperatures



and due to our previous work on switchable catalysts.<sup>43</sup> However, a reduction optimisation study should be performed in the future by considering the structure–activity relationships in order to further improve the DFMs economics. The percentage of CO<sub>2</sub> in the mixture was 10% so as to simulate as far as possible the CO<sub>2</sub> content in post combustion or cement production effluent gas streams.<sup>28</sup> Fig. 4 shows the amount of CO<sub>2</sub> desorbed and the product formation (CH<sub>4</sub>, CO or H<sub>2</sub>) in each reaction for the three DFMs and Fig. S4, S5 and S6† show the volumetric flow rates of all gases vs. time plots of NiRuNa, NiRuK, and NiRuCa, respectively.

Fig. 4 reveals the feasibility of switchable DFMs, where 100% selectivity in conversion of captured CO<sub>2</sub> to either methane or CO is obtained for all 3 cases (methanation, RWGS and DRM) and for all DFMs investigated herein. In all cases, the CO<sub>2</sub> was captured at the desired temperature and was subsequently converted into CH<sub>4</sub>, CO, and syngas, depending on the temperature and the co-reactant used. It was demonstrated that the formation of by-products *via* side reactions was prevented except for the DRM scenario where DFMs were shown to also catalyse methane cracking once captured CO<sub>2</sub> was consumed. In this case, a surplus of H<sub>2</sub> was obtained which could be useful depending on the envisaged application. A small amount of CO<sub>2</sub> was desorbed during all reactions. However, it appeared that this was not temperature dependent because it was found that approximately the same amount of CO<sub>2</sub> was desorbed in all three reactions. This is interpreted as an indication that some fraction of adsorption sites was not in sufficient proximity with the catalytic sites, and so the adsorbed CO<sub>2</sub> ended up being desorbed. Therefore, there is room for improvement both in material design by fine-

tuning the DFMs nanostructure and in reaction engineering by adding another catalyst bed to convert the residual CO<sub>2</sub> or improving mass transfer by reactor design, for instance, by using microchannel reactors or micro-monoliths.<sup>58,59</sup> No CO<sub>2</sub> was detected during the heating ramp between methanation and RWGS, demonstrating that the entire amount of CO<sub>2</sub> adsorbed had either been converted into CH<sub>4</sub> or was desorbed.

It was observed that all DFMs were more active in the DRM reaction compared to RWGS. NiRuK was the best performing DFM in the CO<sub>2</sub> methanation followed by NiRuCa and NiRuNa. In both RWGS and DRM, NiRuCa was the best DFM and after that, it was NiRuK and NiRuNa. It was concluded that the performance of the DFMs strongly depended on the materials basicity and their CO<sub>2</sub> desorption ability at the selected temperature, as observed in the CO<sub>2</sub>-TPD profiles later on. Additionally, it was shown that the proximity of the adsorption and catalytic sites was a more vital parameter compared to the adsorption capacity. This was evident in the case of NiRuNa, which had the highest CO<sub>2</sub> capacity at 350 °C, yet had the worst performance in the CO<sub>2</sub> methanation reaction, indicating an unsatisfactory interaction between the Na and Ni–Ru species. In terms of overall performance, DFMs can be ranked in the order NiRuCa > NiRuK > NiRuNa.

In terms of product signals, as observed in Fig. S4–S6,† an initial spike in the products was detected, demonstrating a fast reaction between the captured CO<sub>2</sub> and the excess co-reactant (H<sub>2</sub> or CH<sub>4</sub>), followed by a slower decrease in their signals. Additionally, it was observed that the reactions took place in the first 10 minutes, allowing space for further optimisation of the process by minimising the reaction time. It is worth noting, however, that in order for two reactors to run in paral-



Fig. 4 Results of feasibility study of flexible DFMs, showing the amount of CO<sub>2</sub> desorbed and products formation in each reaction for NiRuNa, NiRuK and NiRuCa.



lel in the DFM technology, the CO<sub>2</sub> capture and reduction steps need to have the same duration and if this is not the case, alternative configurations are required. Typically, in adsorption systems, regeneration is the slow step that necessitates boosting *via* temperature or pressure swing. Therefore, the fast reaction (which is also regeneration) time observed in DFMs is a major advantage for designing industrially applicable systems.

An interesting finding was that of the CO formation during the capture steps, an indication that CO<sub>2</sub> may have been reduced by Ce<sup>3+</sup>, or even by Ni and Ru species, leading to CO formation and Ce<sup>4+</sup>. These species were re-reduced when H<sub>2</sub> was either flowing or being generated in the subsequent steps.<sup>35,41</sup> This would in turn mean that the materials were able to sequentially be oxidised and reduced throughout the duration of the experiment without any structure alteration, as shown by the post-characterisation of the spent materials. Another explanation for the CO formation during the capture step would have been the occurrence of the reverse Boudouard reaction between the CO<sub>2</sub> and some carbon species, resulting in CO production. The occurrence of RWGS between the available CO<sub>2</sub> and the chemisorbed H<sub>2</sub> could not be excluded too, as only a small amount of CO was formed during the CO<sub>2</sub> capture step at 350 °C, which was not the case at 650 °C. In addition to the CO formation, there was an amount of H<sub>2</sub> produced during the capture step. This might have happened because of H<sub>2</sub> being chemisorbed in a previous step, and thus being displaced by CO<sub>2</sub>. Alternatively, H<sub>2</sub> might have been produced from the oxidation of Ce<sup>3+</sup> species with some leftover H<sub>2</sub>O species coming from previous reactions including the initial DFMs reduction, CO<sub>2</sub> methanation and RWGS. Due to the increased complexity of these materials, further mechanistic studies are required to verify exact mechanisms and based on their results, optimisation and redesign of such experiments can take place in the future. In particular, it is necessary to test DFMs also under real flue gas and active direct air capture conditions to assess their performance for a range of realistic applications. In this study, we show that the DFMs passively capture CO<sub>2</sub> from the ambient air and are able to convert it into CH<sub>4</sub> or syngas *via* CO<sub>2</sub> methanation and DRM respectively, which is a strong indication that they can tolerate oxygen and some moisture.

By observing the CO and H<sub>2</sub> profiles of the NiRuNa during RWGS, an unexpected result emerged. It appeared that even when no CO and H<sub>2</sub> were produced during that reaction, the H<sub>2</sub> signal decreased and no CH<sub>4</sub> was formed. However, during the subsequent CO<sub>2</sub> capture step, these gases were indeed detected. Therefore, it was assumed that there had not been enough heat produced during that step so as to release the products of the endothermic RWGS. Once a small amount of heat was produced during the next exothermic adsorption step, these gases were able to be released, and thus detected by the gas analyser. As a result, the DFM's sites were once again free to adsorb CO<sub>2</sub> during the capture step.

During DRM, the DFMs were able to initially convert the captured CO<sub>2</sub> into syngas, as illustrated by the CO and H<sub>2</sub>

signals. However, methane cracking was observed for all DFMs as a significant amount of CH<sub>4</sub> was used and H<sub>2</sub> was produced. This was anticipated because the captured CO<sub>2</sub> had initially been converted into syngas and, as time went by and its availability was limiting, the CH<sub>4</sub> was decomposed into carbon and H<sub>2</sub>. This phenomenon had already been reported during the post-breakthrough stage.<sup>39</sup> As a result, the H<sub>2</sub>/CO ratio was higher than its stoichiometric value of 1 and a H<sub>2</sub> rich syngas was produced, which could be useful in CO<sub>2</sub> applications that require a higher H<sub>2</sub>/CO ratio. A good strategy for limiting the carbon formation would have been to decrease the DRM duration, as it had taken place predominantly in the first 5 to 10 minutes, because allowing this step to occur for longer would serve no purpose. In a realistic scenario, the stoichiometric amount of CH<sub>4</sub> would have been added to the system based on the CO<sub>2</sub> uptake to control the ratio of CO<sub>2</sub> and CH<sub>4</sub>. In general, as CH<sub>4</sub> cracking was observed after DRM reaction (Fig. S4–S6†), pulsing a controllable amount of CH<sub>4</sub> to minimise the extent of cracking and coke formation would have been the way forward from an engineering perspective. Nevertheless, previous reports<sup>38–40</sup> demonstrated that the carbon formed during the DRM reaction was able to be regenerated during the subsequent CO<sub>2</sub> capture step *via* the endothermic reverse Boudouard reaction. The occurrence of the reverse Boudouard reaction would have been expected for these materials too if a CO<sub>2</sub> capture step had occurred after the DRM step.

Table 3 shows a comparative analysis of these switchable DFMs with similar materials in literature.<sup>28</sup> It can be observed that the designed DFMs of this work have similar performance to the ones in literature who were prepared by the same synthesis method, impregnation. Hence, studies that directly compare the various DFMs synthesis methods should be carried out, with an emphasis on understanding the structure–activity relationships. It is worth mentioning that in this work, a longer N<sub>2</sub> purge step had been carried out in between the CO<sub>2</sub> capture and reaction steps compared to other studies, which definitely had decreased the product formation. However, this took place just to confirm the spill over mechanism of DFMs and their ability to convert the adsorbed CO<sub>2</sub> into various products. So, this is not how the DFM technology would necessarily work in industry, although a N<sub>2</sub> purge step would potentially be needed when O<sub>2</sub>-containing CO<sub>2</sub> capture feed would be used to avoid the mixing of O<sub>2</sub> and H<sub>2</sub>. Besides fine-tuning the synthesis method of DFMs, reaction engineering optimisation, design and technoeconomic assessment are also necessary to scale up DFMs.

### 3.2. Characterisation

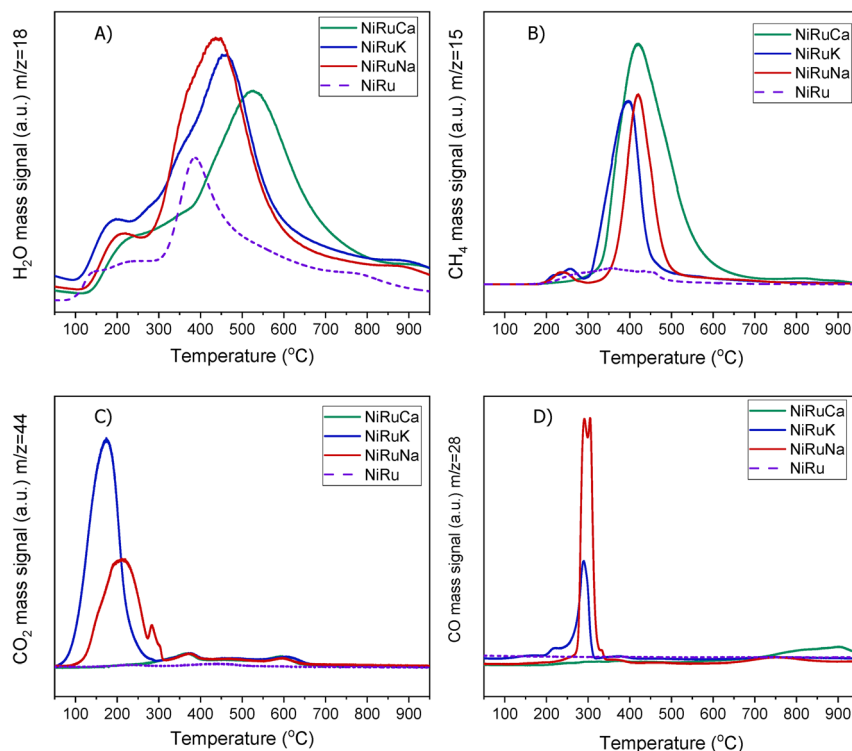
**3.2.1 Reducibility profiles H<sub>2</sub>-TPR and evidence of passive direct air capture.** The reduction properties and interaction between the species of the supported adsorbents and the DFMs were observed in the H<sub>2</sub>-TPR studies. Fig. S7† shows the H<sub>2</sub> signals of the DFMs and Fig. 5 the CH<sub>4</sub>, H<sub>2</sub>O, CO and CO<sub>2</sub> signals (*m/z* = 15, 18, 28, 44) recorded during the





**Table 3** Summary of DFMs performance data and comparison of similar DFMs from literature

DFM	Reaction temperature (°C)	Product formation ( $\mu\text{mol g}_{\text{DFM}}^{-1}$ )	Ref.
15% Ni–1%Ru, 10% Na <sub>2</sub> O/CeO <sub>2</sub> –Al <sub>2</sub> O <sub>3</sub>	350	Meth. CH <sub>4</sub> : 87	This work
	650	RWGS CO: 2	
	650	DRM CO: 153	
15% Ni–1% Ru, 10% K <sub>2</sub> O/CeO <sub>2</sub> –Al <sub>2</sub> O <sub>3</sub>	350	DRM H <sub>2</sub> : 25 774	This work
	650	Meth. CH <sub>4</sub> : 153	
	650	RWGS CO: 13	
	650	DRM CO: 239	
15% Ni–1% Ru, 10% CaO/CeO <sub>2</sub> –Al <sub>2</sub> O <sub>3</sub>	350	DRM H <sub>2</sub> : 22 512	This work
	650	Meth. CH <sub>4</sub> : 104	
	650	RWGS CO: 58	
	650	DRM CO: 338	
1% Ru–10% Ni, 10% Na <sub>2</sub> CO <sub>3</sub> /Al <sub>2</sub> O <sub>3</sub>	350	DRM H <sub>2</sub> : 32 639	56
	550	Meth. CH <sub>4</sub> : 266	
1% Ce–10% Ni, 10% Na <sub>2</sub> CO <sub>3</sub> /Al <sub>2</sub> O <sub>3</sub>	350	Meth. CH <sub>4</sub> : 145	56
	550	Meth. CH <sub>4</sub> : 172	
1% Ru–10% Ni, 6.1% “Na <sub>2</sub> O”/Al <sub>2</sub> O <sub>3</sub>	350	Meth. CH <sub>4</sub> : 125	25
	320	Meth. CH <sub>4</sub> : 280	
5% Ru, 10% CaO/Al <sub>2</sub> O <sub>3</sub>	320	Meth. CH <sub>4</sub> : 500	24
5% Ru, 10% Na <sub>2</sub> CO <sub>3</sub> /Al <sub>2</sub> O <sub>3</sub>	320	Meth. CH <sub>4</sub> : 1050	27
5% Ru, 6.1% “Na <sub>2</sub> O”/CeO <sub>2</sub>	320	Meth. CH <sub>4</sub> : 320	57
5% Ru, 7.01% “K <sub>2</sub> O”/Al <sub>2</sub> O <sub>3</sub>	320	Meth. CH <sub>4</sub> : 467	57
Ni/CaO	500	Meth. CH <sub>4</sub> : 13 500	41
	700	RWGS CO: 400	
	700	DRM CO: 20 200	
Ca <sub>1</sub> Ni <sub>0.1</sub> Ce <sub>0.033</sub>	650	DRM H <sub>2</sub> : 131 700	35
		RWGS CO: 7300	

**Fig. 5** H<sub>2</sub>-TPR study for NiRuNa, NiRuK, NiRuCa and NiRu: (A) H<sub>2</sub>O, (B) CH<sub>4</sub>, (C) CO<sub>2</sub> and (D) CO signals.

H<sub>2</sub>-TPR experiments. In Fig. 5, NiRu switchable catalyst, which we developed previously,<sup>43</sup> was used as a reference material.

A striking finding was the detection of CO and CH<sub>4</sub> in the DFMs compared to the NiRu catalyst, as seen in Fig. 5B and D. By looking at the CO<sub>2</sub>, H<sub>2</sub>O, and H<sub>2</sub> signals, besides the CH<sub>4</sub>, it



can be seen that after their synthesis, all DFMs synthesised in this work were able to adsorb CO<sub>2</sub> directly and passively from the atmospheric air and convert it into CH<sub>4</sub> via the CO<sub>2</sub> methanation reaction. CO formation was also observed on NiRuK and NiRuNa. Therefore, Ni and Ru, which were already reduced by these temperatures (*i.e.* 440 °C for NiRuNa, 455 °C for NiRuK, and 520 °C for NiRuCa) were used to produce CH<sub>4</sub> and H<sub>2</sub>O from the atmospheric CO<sub>2</sub> captured on adsorbent sites using the H<sub>2</sub> feed during the H<sub>2</sub>-TPR study. Desorption of CO<sub>2</sub> and generation of other products of CO<sub>2</sub> reduction were also detected mainly at low temperatures, in agreement with the CO<sub>2</sub>-TPD results and the different types of basic sites, as presented later. Consequently, the main peak of the DFMs in the H<sub>2</sub>O signal profiles corresponded to the H<sub>2</sub>O from the methanation reaction, holding promise for using DFMs for flexible chemicals synthesis from CO<sub>2</sub> in the air.

As seen in Fig. S7,† which presented similar peaks to the H<sub>2</sub>O signal, the NiRuNa and NiRuK samples had a similar pattern since three distinct peaks were observed. The NiRuCa sample showed a broader reduction pattern up to 350 °C, but two peaks were seen over that temperature. By observing the H<sub>2</sub>O signals of the three DFMs in Fig. 5A, it can be seen that the first peak at 200 °C corresponded to the reduction of Ru<sup>4+</sup> to metallic Ru. These were located at a higher temperature compared to the reference material, indicating a better interaction of the Ru species with the other species.<sup>60</sup> Moreover, a broad reduction zone located at 440 °C for the NiRuNa, another at 455 °C for the NiRuK, and another one at 520 °C for the NiRuCa were detected. In all those reduction events, a shoulder at the lower temperature range was displayed, attributed to the medium-sized NiO<sub>x</sub> species interacting with the CeO<sub>2</sub> particles.<sup>61,62</sup> The slow decrease of the signal over 800 °C corresponded to the reduction of a small amount of bulk CeO<sub>2</sub> species,<sup>63</sup> confirming the reduced XRD profiles, which showed that surface CeO<sub>2</sub> species were the main CeO<sub>2</sub> species in the samples.

**3.2.2. Basicity profiles CO<sub>2</sub>-TPD.** The CO<sub>2</sub>-TPD was used to assess the basicity of the supported adsorbents and DFMs. In a CO<sub>2</sub>-TPD profile (Fig. 6), different types of basic sites are observed, which can be categorised into weak, medium, and strong ones. Weak basic sites are characterised by CO<sub>2</sub> desorp-

tion up to 250 °C, while medium basic sites are characterised by CO<sub>2</sub> desorption between 250 °C and 700 °C. Finally, the strong basic sites result in stable adsorption of CO<sub>2</sub> and are characterised by desorption temperatures exceeding 700 °C.<sup>50,64</sup> The strength of basic sites is an important descriptor for designing switchable DFMs because it provides insight into available reactant species at different temperature ranges that can be used for CO<sub>2</sub> methanation, RWGS and DRM. In other words, weak basic sites can be beneficial for CO<sub>2</sub> methanation, while medium basic sites for RWGS and DRM.

Fig. 6 demonstrates the CO<sub>2</sub>-TPD results of DFMs and supported adsorbents, while Fig. S8† shows the corresponding results of the reference Ni–Ru switchable catalyst. All the materials displayed mainly weak and medium basic sites. By comparing the DFMs with the NiRu catalyst, it was noted that the addition of the adsorbents contributed to the formation of medium basic sites. Therefore, it was shown that the adsorbents were in a dispersed form rather than bulk species, meaning that the DFMs would behave like intermediate-temperature adsorbents and reversibly adsorb CO<sub>2</sub> at intermediate temperatures in agreement with literature.<sup>65</sup> Although the CO<sub>2</sub>-TPD profiles of the DFMs had been mainly influenced by the supported adsorbents, by comparing the DFMs and supported adsorbents profiles, it was observed that the addition of Ni and Ru to the supported adsorbents suppressed the medium basic sites. This meant that, to some extent, Ni and Ru covered a small amount of adsorption sites during impregnation.<sup>50</sup> Although NiRuK displayed a higher intensity signal for medium basic sites (300–700 °C) than NiRuNa, the CO<sub>2</sub>-TPD profiles of these materials were similar to each other. As regards the NiRuCa sample, a different profile was observed with a smaller amount of weak basic sites and more medium-strong ones, in agreement with its CO<sub>2</sub> signal profile in the H<sub>2</sub>-TPR study as well as the TGA study at high temperatures.

**3.2.3. CH<sub>4</sub>-TPSR and evidence of passive direct air capture.** Furthermore, a CH<sub>4</sub>-TPSR experiment was carried out on the best performing DFM, NiRuCa. Its aim was to observe the fresh DFM performance in a CH<sub>4</sub> environment, similar to the H<sub>2</sub>-TPR experiment, and identify opportunities for a potential temperature reduction of the high-temperature reactions. This would ultimately be translated into lower energy requirement,

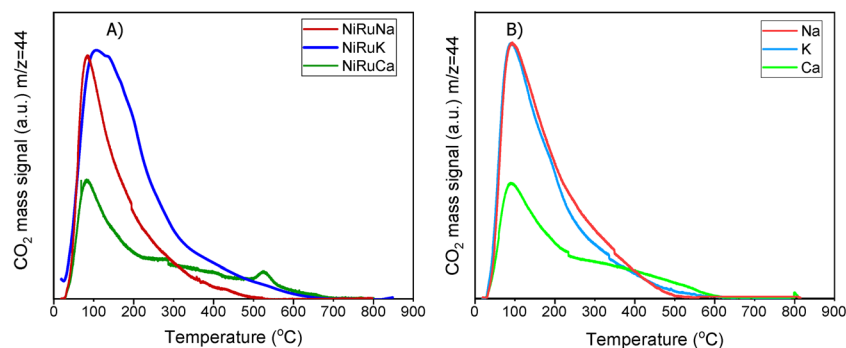


Fig. 6 CO<sub>2</sub>-TPD profiles of the (A) DFMs and (B) supported adsorbents.



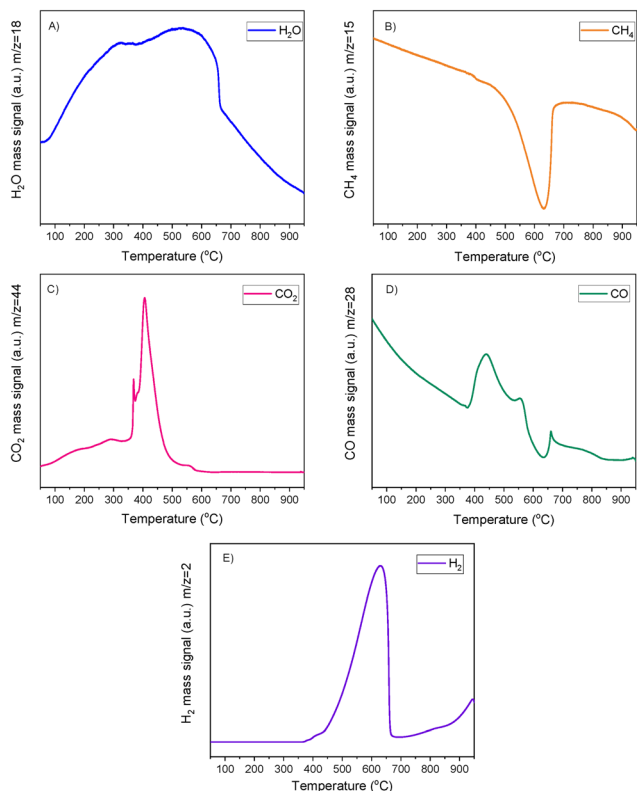


Fig. 7 CH<sub>4</sub>-TPSR profile of NiRuCa: (A) H<sub>2</sub>O, (B) CH<sub>4</sub>, (C) CO<sub>2</sub>, (D) CO and (E) H<sub>2</sub> signals.

minimising the operating costs in a potential scale-up of the switchable DFMs.

Fig. 7 shows the CH<sub>4</sub>-TPSR results. Overall, it was demonstrated that the DFM's oxidation (since the sample used was after calcination) did not shut down its activity for DRM which was remarkable. In agreement with the H<sub>2</sub>-TPR results, atmospheric CO<sub>2</sub> was adsorbed onto the DFM and was gradually released until a peak at 400 °C was observed. A peak at higher temperature analogous to the H<sub>2</sub>-TPR and CO<sub>2</sub>-TPD results was not identified, meaning that CO<sub>2</sub> was fully consumed during low temperature reaction. A CO peak was also seen at this temperature (400 °C). Additionally, CH<sub>4</sub> cracking took place starting at 350–400 °C and peaked at 635 °C, as observed from the H<sub>2</sub> and CH<sub>4</sub> signals. Therefore, it was shown that in a CH<sub>4</sub>-rich environment and in the temperature range of 400–600 °C, CH<sub>4</sub> cracking supplied the H<sub>2</sub> needed for the reduction of Ni and Ru which was feasible at these temperatures. Thus, DRM was able to take place because of the available CH<sub>4</sub> and atmospheric CO<sub>2</sub>. However, after the consumption of CO<sub>2</sub>, excessive CH<sub>4</sub> cracking took place, which was expected based on our isothermal experiment results shown in section 3.1.2. It is worth mentioning that RWGS and reverse Boudouard reactions could also be responsible for some CO formation as well.

Based on these results, it was confirmed that a DRM temperature reduction to 400 °C could be feasible. It may also be possible to lower the temperature of DRM using other driving

forces for reaction.<sup>66,67</sup> It should be kept in mind that the DFMs operate under dynamic conditions, meaning that a deviation from the well-known steady state conditions is possible. A significant RWGS temperature reduction would require a catalyst that is not active for the methanation reaction, thus being beyond the aim of the present study which focuses on switchable performance with 100% selectivity depending on reaction conditions. As CO<sub>2</sub> methanation and RWGS have the same reactants, the reaction parameter changed to achieve a different product formation is temperature. So, if the RWGS temperature is significantly reduced, then 100% CO selectivity may not be achieved. The initial temperature of RWGS and DRM, *i.e.* 650 °C was considered useful for this validation study since higher temperatures are more representative of the current industrial reformers that operate close to equilibrium conversions at 900–1000 °C.<sup>68</sup> However, investigating the DFM behaviour at a temperature higher than 650 °C was considered to be unnecessary, because the DFMs had 100% selectivity in these reactions. In fact, it would have had a negative effect due to reduced CO<sub>2</sub> adsorption and sintering, let alone the increase of operating costs in a potential scale up.

**3.2.4. Textural properties.** The textural properties of the supported adsorbents and DFMs and the N<sub>2</sub> adsorption–desorption isotherms of these materials are presented in Fig. 8. There appear to be no substantial differences between the BET surface areas, pore volumes and pore diameters when comparing adsorbents and DFMs. As regards to the isotherms generated, they corresponded to the type IV isotherms with a characteristic H1 hysteresis loop, according to IUPAC classification. This type of isotherm is linked to well-developed cylindrical mesoporous materials and the high steepness was indicative of the mesopores being homogeneously distributed throughout the structure of the samples,<sup>69,70</sup> as observed in SEM and TEM as well.

**3.2.5. Crystalline structure.** Fig. 9 shows the crystalline phases of the fresh materials. All the supported adsorbents and DFMs had the characteristic peaks of  $\gamma$ -Al<sub>2</sub>O<sub>3</sub> and CeO<sub>2</sub> phases (JCPDS 00-004-0880 and JCPDS 03-065-5923, respectively). CaO, K<sub>2</sub>O and Na<sub>2</sub>O peaks were not observed, indicating that these species were likely present as amorphous and/or highly dispersed phases.<sup>71,72</sup> In the fresh Na, K, and NiRuNa samples, some residual nitrates peaks were observed, which eventually disappeared upon reduction, as seen in Fig. 10. In the fresh DFM XRD patterns, the peaks located at  $2\theta = 37.2^\circ$ ,  $43.3^\circ$ ,  $62.9^\circ$ , and  $75.4^\circ$  (JCPDS 00-047-1049) were ascribed to NiO. The existence of nickel aluminate (NiAl<sub>2</sub>O<sub>4</sub>) spinels was discarded due to the low calcination temperature used.<sup>56</sup> Peaks of RuO<sub>2</sub> were also observed in the fresh samples (JCPDS 01-070-2662). No evidence of a Ni–Ru alloy was detected in the fresh DFMs.

Upon reduction at 800 °C, as observed in Fig. 10, the CeO<sub>2</sub> peaks either disappeared or were significantly lower in intensity. As a result, it was concluded that surface CeO<sub>2</sub> species were mainly present in the samples, which was in agreement with the H<sub>2</sub>-TPR results presented previously for Ce–Al supported catalysts.<sup>73</sup> No ceria aluminate (CeAlO<sub>3</sub>) species were



Sample	$S_{\text{BET}}$ ( $\text{m}^2/\text{g}$ )	$V_{\text{PORE}}$ ( $\text{cm}^3/\text{g}$ )	$D_{\text{PORE}}$ (nm)
Na	109	0.29	10.5
K	136	0.36	10.4
Ca	170	0.39	8.7
NiRuNa	173	0.41	9.4
NiRuK	170	0.40	8.9
NiRuCa	194	0.37	6.9



Fig. 8 Textural properties of the materials on the left-hand side and nitrogen adsorption–desorption isotherms of the (A) supported adsorbents and (B) DFMs on the right-hand side.



Fig. 9 XRD patterns of the fresh (A) supported adsorbents and (B) DFMs.

seen, which is consistent with the use of a reduction temperature of 800 °C.<sup>69</sup> Metallic Ni peaks were also detected in the reduced DFM XRD patterns (JCPDS 01-070-1849). In contrast, metallic Ru peaks were not observed, which led us to believe that Ru was well dispersed and/or a Ni–Ru alloy was formed; however, due to the low Ru weight content (1 wt%) compared to Ni (15 wt%), no shift of Ni peaks could be discerned in the XRD patterns.<sup>21,74</sup>

**3.2.6. Morphological structure.** The morphological structure of the fresh supported adsorbents and the DFMs was observed in SEM. Fig. S9–S14<sup>†</sup> showed that after calcination,

the materials presented porous structure, which was in accordance with the BET results. The EDX mappings of the DFMs are shown in Fig. 11–13 and of the supported adsorbents in Fig. S15–S17.<sup>†</sup> The EDX mapping indicated that the materials were successfully impregnated as dispersed and homogenous materials were created. The high dispersion, porosity, and homogeneity of the DFMs were significant parameters that contributed to their impressive performance, as described earlier, due to the need to have a plethora of adsorption and catalytic sites in close proximity in order for them to work efficiently.<sup>24,75</sup>





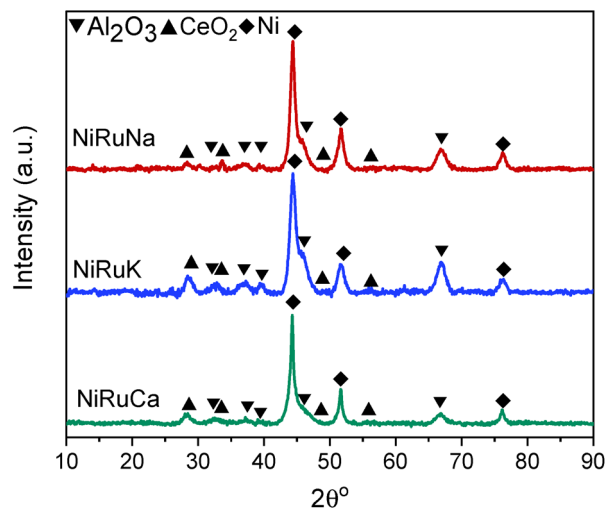


Fig. 10 XRD patterns of reduced DFMs.

Additionally, TEM images of the three reduced DFMs are presented in Fig. 14. These images revealed the nanostructure of these materials with Ni and Ru having a particle diameter of less than 10 nm overall. In general, a good dispersion of their active catalytic phases was achieved in accordance with their EDX profiles.

### 3.3. Post reaction characterisation

As shown in Fig. S4–S6,† CH<sub>4</sub> cracking took place in the feasibility study of the switchable DFMs that resulted in the formation of coke, and hence XRD and TGA were carried out on the spent catalysts to characterise and quantify the carbon species.

Fig. 15 shows the XRD patterns of the post-reaction NiRuNa, NiRuK, and NiRuCa samples. The patterns were similar to their reduced ones presented in Fig. 10, displaying the characteristic peaks of Ni, CeO<sub>2</sub>, and Al<sub>2</sub>O<sub>3</sub>. No carbon peak was observed in the spent NiRuNa and NiRuK XRD profiles, meaning that the type of carbon formed was soft with a poorer degree of crystallinity. However, this was not the case with the NiRuCa, as a carbon peak at  $2\theta = 26$  was observed, signifying the formation of a harder carbon potentially requiring higher regeneration temperatures. A slight shift of the Ni peak to lower angles appeared on the NiRuNa and NiRuCa samples indicating the formation of a NiRu alloy, which was not the case with their reduced materials.<sup>21</sup> Hence, it was concluded that a NiRu alloy was formed during reduction even though it was not evident from their XRD patterns. Such alloy plays a key role in the catalytic conversion process.

Thermogravimetric analysis during temperature programmed oxidation (TPO) was also used to quantify the carbon formed on post-reaction DFMs after the feasibility

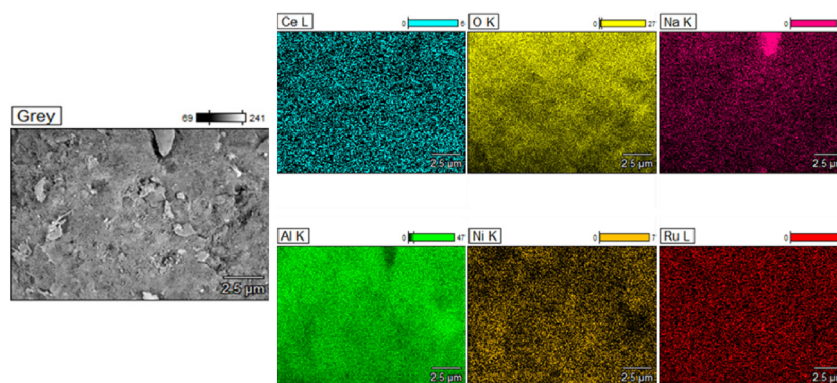


Fig. 11 SEM and EDX mapping of NiRuNa.



Fig. 12 SEM and EDX mapping of NiRuK.





Fig. 13 SEM and EDX mapping of NiRuCa.



Fig. 14 TEM images of (A) NiRuNa, (B) NiRuK and (C) NiRuCa.



Fig. 15 XRD for post reaction NiRuNa, NiRuK and NiRuCa.



Fig. 16 TGA for reduced and post reaction NiRuNa, NiRuK and NiRuCa samples.

testing, especially expected from the performance during the DRM step. In order to accurately measure the amount of carbon, *ex situ* reduced DFMs were also tested under the same conditions. Therefore, the weight loss due to the atmospheric CO<sub>2</sub> and moisture adsorption and material degradation, as well as the weight gain due to the oxidation of the materials, were also taken into account. The results are presented in

Fig. 16. In all the samples, an initial weight loss took place up to 200–300 °C because of the weakly adsorbed atmospheric CO<sub>2</sub> and moisture. A higher weight loss was seen in the reduced materials because they were able to absorb a higher amount of atmospheric impurities. Moreover, a weight gain was observed at the 300–400 °C temperature range, which was associated with the oxidation of the remaining Ni and Ru particles. At temperatures higher than 400 °C, a significant weight



loss was detected, showing the carbon oxidation. The coke oxidation was completed by 500 °C for the NiRuNa and NiRuK samples, while a higher temperature was needed for the NiRuCa sample, confirming the existence of softer carbon species in the former samples and of harder ones in the latter. The formation of soft carbon was an intriguing result as it will likely allow an easier regeneration process in the future. Overall, the amount of carbon formed during the DRM reaction was 0.083 g<sub>C</sub>/g<sub>sample</sub> for NiRuNa, 0.072 g<sub>C</sub>/g<sub>sample</sub> for NiRuK and 0.075 g<sub>C</sub>/g<sub>sample</sub> for NiRuCa, showing a similar extent of CH<sub>4</sub> cracking for the three DFMs.

## 4. Conclusions

In this work, a series of advanced universal materials for the integrated CO<sub>2</sub> capture and conversion were designed. The combination of an adsorbent and a switchable catalyst led to the development of switchable DFMs that were shown for the first time to be able to capture CO<sub>2</sub> at various temperatures and, depending on the reaction conditions, to convert it into different added-value chemicals through the CO<sub>2</sub> methanation, RWGS, and DRM catalytic upgrading routes. This proof of concept is a milestone in the development of carbon negative technologies to combat the increased CO<sub>2</sub> emissions and the resulting global warming. Switchable DFMs can be adapted to the current infrastructure as a CCU unit, while offering a solution to the highly variable energy sector.

The designed DFMs of this work were highly dispersed and nanostructured porous materials and their species, located in close proximity, showed a high degree of interaction with each other. The H<sub>2</sub>-TPR experiments demonstrated that these materials were able to passively adsorb atmospheric CO<sub>2</sub> through direct air capture and to convert it into synthetic natural gas. The CO<sub>2</sub> adsorption-desorption studies of the selected DFMs surprisingly proved that they were able to reversibly adsorb CO<sub>2</sub> at different temperatures, making them ideal for a flexible DFM scenario. A synergy between the species also took place, contributing to their increased adsorption capacities. Overall, the CO<sub>2</sub> adsorption capacities of the DFMs were in accordance with their basicity profiles, as revealed by the CO<sub>2</sub>-TPD results. NiRuCa was the best DFM, producing 104 μmol of CH<sub>4</sub> per kg<sub>DFM</sub> in CO<sub>2</sub> methanation, 58 μmol of CO per kg<sub>DFM</sub> in RWGS and 338 μmol of CO per kg<sub>DFM</sub> in DRM. It was also concluded that the DFMs displayed a complex CO<sub>2</sub> capture behaviour over different types of adsorption sites, which will necessitate mechanistic studies for understanding their behaviour during DFM operation. CO<sub>2</sub> capture under realistic flue gas conditions with O<sub>2</sub>, steam and SO<sub>2</sub> was out of the scope of this manuscript, even if some degree of oxygen tolerance is expected given their behaviour during H<sub>2</sub>-TPR. Future studies dealing with these impurities similar to literature<sup>76</sup> are highly recommended as a future direction.

The feasibility study of performing CO<sub>2</sub> capture and then either CO<sub>2</sub> methanation, RWGS or DRM reactions was demon-

strated, providing a new tool for devising low emission chemical production schemes in the near term when availability of green hydrogen will be increasing and the demand for different products (such as synthetic natural gas vs. syngas or CO) will be variable. Our findings make it possible to adapt to uncertainty by designing flexible chemical production schemes from CO<sub>2</sub> emissions, whether they are captured from stationary sources or the ambient atmosphere.

## Conflicts of interest

There are no conflicts to declare.

## Author contributions

Loukia-Pantzechroula Merkouri: conceptualisation, methodology, formal analysis, investigation, writing – original draft, visualisation. Tomas Ramirez Reina: conceptualisation, resources, writing – review & editing, supervision, funding acquisition. Melis S. Duyar: conceptualisation, resources, writing – review & editing, supervision, funding acquisition.

## Acknowledgements

Financial support for this work was provided by the Department of Chemical and Process Engineering and the Doctoral College of the University of Surrey. This work was partially sponsored by the European Commission through the H2020-MSCA-RISE-2020 BIOALL project (Grant Agreement: 101008058). The TEM instrument was funded by EPSRC grant EP/V036327/1. SASOL is kindly acknowledged for providing the CeAl support. The authors would like to acknowledge the help of the department's lab technicians Ben Gibbons, Thomas Chamberlain and Panagiotis Sarikas for their continued support in the lab activities of L.-P. Merkouri. L.-P. Merkouri also thanks Andreas Iakovidis of Mechanical Engineering Sciences and Dr Vlad Stolojan of the Department of Electrical and Electronic Engineering for their assistance with SEM and TEM respectively.

## References

- 1 IEA, Global energy review – CO<sub>2</sub> emissions 2021. <https://www.iea.org/reports/global-energy-review-2021/co2-emissions> (accessed April 4, 2022).
- 2 United Nations Framework Convention on Climate Change. Adoption of the Paris Agreement. Paris, 2015.
- 3 J. Rogelj, M. Den Elzen, N. Höhne, T. Fransen, H. Fekete, H. Winkler, *et al.*, Paris Agreement climate proposals need a boost to keep warming well below 2 °C, *Nature*, 2016, **534**, 631–639, DOI: [10.1038/nature18307](https://doi.org/10.1038/nature18307).
- 4 J. C. M. Pires, F. G. Martins, M. C. M. Alvim-Ferraz and M. Simões, Recent developments on carbon capture and





- storage: An overview, *Chem. Eng. Res. Des.*, 2011, **89**, 1446–1460, DOI: [10.1016/j.cherd.2011.01.028](#).
- 5 A. Samanta, A. Zhao, G. K. H. Shimizu, P. Sarkar and R. Gupta, Post-combustion CO<sub>2</sub> capture using solid sorbents: A review, *Ind. Eng. Chem. Res.*, 2012, **51**, 1438–1463, DOI: [10.1021/ie200686q](#).
  - 6 K. Damen, M. V. Troost, A. Faaij and W. Turkenburg, A comparison of electricity and hydrogen production systems with CO<sub>2</sub> capture and storage. Part A: Review and selection of promising conversion and capture technologies, *Prog. Energy Combust. Sci.*, 2006, **32**, 215–246, DOI: [10.1016/j.pecs.2005.11.005](#).
  - 7 A. B. Rao and E. S. Rubin, A technical, economic, and environmental assessment of amine-based CO<sub>2</sub> capture technology for power plant greenhouse gas control, *Environ. Sci. Technol.*, 2002, **36**, 4467–4475, DOI: [10.1021/es0158861](#).
  - 8 A. Al-Mamoori, A. Krishnamurthy, A. A. Rownaghi and F. Rezaei, Carbon Capture and Utilization Update, *Energy Technol.*, 2017, **5**, 834–849, DOI: [10.1002/ente.201600747](#).
  - 9 M. K. Mondal, H. K. Balsora and P. Varshney, Progress and trends in CO<sub>2</sub> capture/separation technologies: A review, *Energy*, 2012, **46**, 431–441, DOI: [10.1016/j.energy.2012.08.006](#).
  - 10 W. Wang, S. Wang, X. Ma and J. Gong, Recent advances in catalytic hydrogenation of carbon dioxide, *Chem. Soc. Rev.*, 2011, **40**, 3703–3727, DOI: [10.1039/c1cs15008a](#).
  - 11 A. T. Najafabadi, CO<sub>2</sub> chemical conversion to useful products: An engineering insight to the latest advances toward sustainability, *Int. J. Energy Res.*, 2013, **37**, 485–499, DOI: [10.1002/er](#).
  - 12 E. le Saché and T. R. Reina, Analysis of Dry Reforming as direct route for gas phase CO<sub>2</sub> conversion. The past, the present and future of catalytic DRM technologies, *Prog. Energy Combust. Sci.*, 2022, **89**, DOI: [10.1016/j.pecs.2021.100970](#).
  - 13 D. Pakhare and J. Spivey, A review of dry (CO<sub>2</sub>) reforming of methane over noble metal catalysts, *Chem. Soc. Rev.*, 2014, **43**, 7813–7837, DOI: [10.1039/c3cs60395d](#).
  - 14 M. C. J. Bradford and M. A. Vannice, CO<sub>2</sub> reforming of CH<sub>4</sub>, *Catal. Rev. - Sci. Eng.*, 1999, **41**, 1–42, DOI: [10.1081/CR-100101948](#).
  - 15 M. Usman, W. M. A. Wan Daud and H. F. Abbas, Dry reforming of methane: Influence of process parameters - A review, *Renewable Sustainable Energy Rev.*, 2015, **45**, 710–744, DOI: [10.1016/j.rser.2015.02.026](#).
  - 16 M. Liu, Y. Yi, L. Wang, H. Guo and A. Bogaerts, Hydrogenation of carbon dioxide to value-added chemicals by heterogeneous catalysis and plasma catalysis, *Catalysts*, 2019, **9**, 275, DOI: [10.3390/catal9030275](#).
  - 17 H. Yang, Z. Xu, M. Fan, R. Gupta, R. B. Slimane, A. E. Bland, *et al.*, Progress in carbon dioxide separation and capture: A review, *J. Environ. Sci.*, 2008, **20**, 14–27, DOI: [10.1016/S1001-0742\(08\)60002-9](#).
  - 18 Y. A. Daza and J. N. Kuhn, CO<sub>2</sub> conversion by reverse water gas shift catalysis: Comparison of catalysts, mechanisms and their consequences for CO<sub>2</sub> conversion to liquid fuels, *RSC Adv.*, 2016, **6**, 49675–49691, DOI: [10.1039/c6ra05414e](#).
  - 19 Q. Zhang, L. Pastor-Pérez, S. Gu and T. R. Reina, Transition metal carbides (TMCS) catalysts for gas phase CO<sub>2</sub> upgrading reactions: A comprehensive overview, *Catalysts*, 2020, **10**, 1–23, DOI: [10.3390/catal10090955](#).
  - 20 P. Frontera, A. Macario, M. Ferraro and P. L. Antonucci, Supported catalysts for CO<sub>2</sub> methanation: A review, *Catalysts*, 2017, **7**, 1–28, DOI: [10.3390/catal7020059](#).
  - 21 F. Lange, U. Armbruster and A. Martin, Heterogeneously-Catalyzed Hydrogenation of Carbon Dioxide to Methane using RuNi Bimetallic Catalysts, *Energy Technol.*, 2015, **3**, 55–62, DOI: [10.1002/ente.201402113](#).
  - 22 R. M. Bown, M. Joyce, Q. Zhang, T. R. Reina and M. S. Duyar, Identifying Commercial Opportunities for the Reverse Water Gas Shift Reaction, *Energy Technol.*, 2021, **9**, 2100554, DOI: [10.1002/ente.202100554](#).
  - 23 J. Gao, Q. Liu, F. Gu, B. Liu, Z. Zhong and F. Su, Recent advances in methanation catalysts for the production of synthetic natural gas, *RSC Adv.*, 2015, **5**, 22759–22776, DOI: [10.1039/c4ra16114a](#).
  - 24 M. S. Duyar, M. A. A. Treviño and R. J. Farrauto, Dual function materials for CO<sub>2</sub> capture and conversion using renewable H<sub>2</sub>, *Appl. Catal., B*, 2015, **168–169**, 370–376, DOI: [10.1016/j.apcatb.2014.12.025](#).
  - 25 M. A. Arellano-Treviño, N. Kanani, C. W. Jeong-Potter and R. J. Farrauto, Bimetallic catalysts for CO<sub>2</sub> capture and hydrogenation at simulated flue gas conditions, *Chem. Eng. J.*, 2019, **375**, 121953, DOI: [10.1016/j.cej.2019.121953](#).
  - 26 S. Wang, E. T. Schruk, H. Mahajan and R. J. Farrauto, The role of ruthenium in CO<sub>2</sub> capture and catalytic conversion to fuel by dual function materials (DFM), *Catalysts*, 2017, **7**, 1–13, DOI: [10.3390/catal7030088](#).
  - 27 M. S. Duyar, S. Wang, M. A. Arellano-Treviño and R. J. Farrauto, CO<sub>2</sub> utilization with a novel dual function material (DFM) for capture and catalytic conversion to synthetic natural gas: An update, *J. CO<sub>2</sub> Util.*, 2016, **15**, 65–71, DOI: [10.1016/j.jcou.2016.05.003](#).
  - 28 L. P. Merkouri, T. R. Reina and M. S. Duyar, Closing the Carbon Cycle with Dual Function Materials, *Energy Fuels*, 2021, **35**, 19859–19880, DOI: [10.1021/acs.energyfuels.1c02729](#).
  - 29 P. Melo Bravo and D. P. Debecker, Combining CO<sub>2</sub> capture and catalytic conversion to methane, *Waste Disposal and Sustainable Energy*, 2019, **1**, 53–65, DOI: [10.1007/s42768-019-00004-0](#).
  - 30 I. S. Omodolor, H. O. Otor, J. A. Andonegui, B. J. Allen and A. C. Alba-Rubio, Dual-Function Materials for CO<sub>2</sub> Capture and Conversion: A Review, *Ind. Eng. Chem. Res.*, 2020, **59**, 17612–17631, DOI: [10.1021/acs.iecr.0c02218](#).
  - 31 S. Sun, H. Sun, P. T. Williams and C. Wu, Recent advances in integrated CO<sub>2</sub> capture and utilization: a review, *Sustainable Energy Fuels*, 2021, **5**, 4546–4559, DOI: [10.1039/d1se00797a](#).
  - 32 C. Jeong-Potter and R. Farrauto, Feasibility Study of Combining Direct Air Capture of CO<sub>2</sub> and Methanation at Isothermal Conditions with Dual Function Materials, *Appl. Catal., B*, 2020, 119416, DOI: [10.1016/j.apcatb.2020.119416](#).





- 33 L. Hu and A. Urakawa, Continuous CO<sub>2</sub> capture and reduction in one process: CO<sub>2</sub> methanation over unpromoted and promoted Ni/ZrO<sub>2</sub>, *J. CO<sub>2</sub> Util.*, 2018, **25**, 323–329, DOI: [10.1016/j.jcou.2018.03.013](https://doi.org/10.1016/j.jcou.2018.03.013).
- 34 S. Sun, Z. Lv, Y. Qiao, C. Qin, S. Xu and C. Wu, Integrated CO<sub>2</sub> capture and utilization with CaO-alone for high purity syngas production, *Carbon Capture Sci. Technol.*, 2021, **1**, 100001, DOI: [10.1016/j.cscst.2021.100001](https://doi.org/10.1016/j.cscst.2021.100001).
- 35 H. Sun, J. Wang, J. Zhao, B. Shen, J. Shi, J. Huang, *et al.*, Dual functional catalytic materials of Ni over Ce-modified CaO sorbents for integrated CO<sub>2</sub> capture and conversion, *Appl. Catal., B*, 2019, **244**, 63–75, DOI: [10.1016/j.apcatb.2018.11.040](https://doi.org/10.1016/j.apcatb.2018.11.040).
- 36 L. F. Bobadilla, J. M. Riesco-García, G. Penelás-Pérez and A. Urakawa, Enabling continuous capture and catalytic conversion of flue gas CO<sub>2</sub> to syngas in one process, *J. CO<sub>2</sub> Util.*, 2016, **14**, 106–111, DOI: [10.1016/j.jcou.2016.04.003](https://doi.org/10.1016/j.jcou.2016.04.003).
- 37 B. Shao, G. Hu, K. A. M. Alkebsi, G. Ye, X. Lin, W. Du, *et al.*, Heterojunction-redox catalysts of Fe: XCoYMg<sub>10</sub>CaO for high-temperature CO<sub>2</sub> capture and in situ conversion in the context of green manufacturing, *Energy Environ. Sci.*, 2021, **14**, 2291–2301, DOI: [10.1039/d0ee03320k](https://doi.org/10.1039/d0ee03320k).
- 38 S. Jo, J. H. Lee, J. H. Woo, T.-Y. Kim, H.-J. Ryu, B. Hwang, *et al.*, Coke-promoted Ni/CaO catal-sorbents in the production of cyclic CO and syngas, *Sustainable Energy Fuels*, 2022, **6**, 81–88, DOI: [10.1039/d1se01136g](https://doi.org/10.1039/d1se01136g).
- 39 S. M. Kim, P. M. Abdala, M. Broda, D. Hosseini, C. Copéret and C. Müller, Integrated CO<sub>2</sub> Capture and Conversion as an Efficient Process for Fuels from Greenhouse Gases, *ACS Catal.*, 2018, **8**, 2815–2823, DOI: [10.1021/acscatal.7b03063](https://doi.org/10.1021/acscatal.7b03063).
- 40 S. Tian, F. Yan, Z. Zhang and J. Jiang, Calcium-looping reforming of methane realizes in situ CO<sub>2</sub> utilization with improved energy efficiency, *Sci. Adv.*, 2019, **5**, eaav5077, DOI: [10.1126/sciadv.aav5077](https://doi.org/10.1126/sciadv.aav5077).
- 41 S. B. Jo, J. H. Woo, J. H. Lee, T. Y. Kim, H. I. Kang, S. C. Lee, *et al.*, CO<sub>2</sub> green technologies in CO<sub>2</sub> capture and direct utilization processes: methanation, reverse water-gas shift, and dry reforming of methane, *Sustainable Energy Fuels*, 2020, **4**, 5543–5549, DOI: [10.1039/d0se00951b](https://doi.org/10.1039/d0se00951b).
- 42 A. I. Tsiotsias, N. D. Charisiou, I. V. Yentekakis and M. A. Goula, The Role of Alkali and Alkaline Earth Metals in the CO<sub>2</sub> Methanation Reaction and the Combined Capture and Methanation of CO<sub>2</sub>, *Catalysts*, 2020, **10**, 35, DOI: [10.3390/eccs2020-07567](https://doi.org/10.3390/eccs2020-07567).
- 43 L.-P. Merkouri, E. le Sache, L. Pastor-Perez, M. S. Duyar and T. R. Reina, Versatile Ni-Ru catalysts for gas phase CO<sub>2</sub> conversion : Bringing closer dry reforming, reverse water gas shift and methanation to enable end-products flexibility, *Fuel*, 2022, **315**, 123097, DOI: [10.1016/j.fuel.2021.123097](https://doi.org/10.1016/j.fuel.2021.123097).
- 44 E. Le Saché, L. Pastor-Pérez, B. J. Haycock, J. J. Villora-Picó, A. Sepúlveda-Escribano and T. R. Reina, Switchable Catalysts for Chemical CO<sub>2</sub> Recycling: A Step Forward in the Methanation and Reverse Water-Gas Shift Reactions, *ACS Sustainable Chem. Eng.*, 2020, **8**, 4614–4622, DOI: [10.1021/acssuschemeng.0c00551](https://doi.org/10.1021/acssuschemeng.0c00551).
- 45 Q. Zhang, J. J. Villora-pico, M. Joyce and A. Sepúlveda-escribano, Ni-Phosphide catalysts as versatile systems for gas-phase CO<sub>2</sub> conversion : Impact of the support and evidences of structure-sensitivity, *Fuel*, 2022, **323**, 1–12, DOI: [10.1016/j.fuel.2022.124301](https://doi.org/10.1016/j.fuel.2022.124301).
- 46 K. Chang, H. Zhang, M. J. Cheng and Q. Lu, Application of Ceria in CO<sub>2</sub> Conversion Catalysis, *ACS Catal.*, 2020, **10**, 613–631, DOI: [10.1021/acscatal.9b03935](https://doi.org/10.1021/acscatal.9b03935).
- 47 P. Boldrin, E. Ruiz-Trejo, J. Mermelstein, J. M. Bermúdez Menéndez, T. R. Reina and N. P. Brandon, Strategies for Carbon and Sulfur Tolerant Solid Oxide Fuel Cell Materials, Incorporating Lessons from Heterogeneous Catalysis, *Chem. Rev.*, 2016, **116**, 13633–13684, DOI: [10.1021/acs.chemrev.6b00284](https://doi.org/10.1021/acs.chemrev.6b00284).
- 48 IEA. Global Hydrogen Review 2021 2021. <https://www.iea.org/reports/global-hydrogen-review-2021> (accessed May 4, 2022).
- 49 S. Cimino, F. Boccia and L. Lisi, Effect of alkali promoters (Li, Na, K) on the performance of Ru/Al<sub>2</sub>O<sub>3</sub> catalysts for CO<sub>2</sub> capture and hydrogenation to methane, *J. CO<sub>2</sub> Util.*, 2020, **37**, 195–203, DOI: [10.1016/j.jcou.2019.12.010](https://doi.org/10.1016/j.jcou.2019.12.010).
- 50 A. Bermejo-López, B. Pereda-Ayo, J. A. González-Marcos and J. R. González-Velasco, Ni loading effects on dual function materials for capture and *in situ* conversion of CO<sub>2</sub> to CH<sub>4</sub> using CaO or Na<sub>2</sub>CO<sub>3</sub>, *J. CO<sub>2</sub> Util.*, 2019, **34**, 576–587, DOI: [10.1016/j.jcou.2019.08.011](https://doi.org/10.1016/j.jcou.2019.08.011).
- 51 L. Proaño, E. Tello, M. A. Arellano-Trevino, S. Wang, R. J. Farrauto and M. Cobo, *In situ* DRIFTS study of two-step CO<sub>2</sub> capture and catalytic methanation over Ru, “Na<sub>2</sub>O”/Al<sub>2</sub>O<sub>3</sub> Dual Functional Material, *Appl. Surf. Sci.*, 2019, **479**, 25–30, DOI: [10.1016/j.apsusc.2019.01.281](https://doi.org/10.1016/j.apsusc.2019.01.281).
- 52 L. Proaño, M. A. Arellano-Treviño, R. J. Farrauto, M. Figueredo, C. Jeong-Potter and M. Cobo, Mechanistic assessment of dual function materials, composed of Ru-Ni, Na<sub>2</sub>O/Al<sub>2</sub>O<sub>3</sub> and Pt-Ni, Na<sub>2</sub>O/Al<sub>2</sub>O<sub>3</sub>, for CO<sub>2</sub> capture and methanation by *in situ* DRIFTS, *Appl. Surf. Sci.*, 2020, **533**, 147469, DOI: [10.1016/j.apsusc.2020.147469](https://doi.org/10.1016/j.apsusc.2020.147469).
- 53 L. Pastor-Pérez, E. Le Saché, C. Jones, S. Gu, H. Arellano-Garcia and T. R. Reina, Synthetic natural gas production from CO<sub>2</sub> over Ni-x/CeO<sub>2</sub>-ZrO<sub>2</sub> (x = Fe, Co) catalysts: Influence of promoters and space velocity, *Catal. Today*, 2018, **317**, 108–113, DOI: [10.1016/j.cattod.2017.11.035](https://doi.org/10.1016/j.cattod.2017.11.035).
- 54 T. R. Reina, S. Ivanova, M. A. Centeno and J. A. Odriozola, The role of Au, Cu & CeO<sub>2</sub> and their interactions for an enhanced WGS performance, *Appl. Catal., B*, 2016, **187**, 98–107, DOI: [10.1016/j.apcatb.2016.01.031](https://doi.org/10.1016/j.apcatb.2016.01.031).
- 55 K. Jalama, Carbon dioxide hydrogenation over nickel-, ruthenium-, and copper-based catalysts: Review of kinetics and mechanism, *Catal. Rev. - Sci. Eng.*, 2017, **59**, 95–164, DOI: [10.1080/01614940.2017.1316172](https://doi.org/10.1080/01614940.2017.1316172).
- 56 A. Bermejo-López, B. Pereda-Ayo, J. A. González-Marcos and J. R. González-Velasco, Alternate cycles of CO<sub>2</sub> storage and in situ hydrogenation to CH<sub>4</sub> on Ni-Na<sub>2</sub>CO<sub>3</sub>/Al<sub>2</sub>O<sub>3</sub>: influence of promoter addition and calcination temperature, *Sustainable Energy Fuels*, 2021, **5**, 1194–1210, DOI: [10.1039/d0se01677b](https://doi.org/10.1039/d0se01677b).



- 57 M. A. Arellano-Treviño, Z. He, M. C. Libby and R. J. Farrauto, Catalysts and adsorbents for CO<sub>2</sub> capture and conversion with dual function materials: Limitations of Ni-containing DFMs for flue gas applications, *J. CO<sub>2</sub> Util.*, 2019, **31**, 143–151, DOI: [10.1016/j.jcou.2019.03.009](https://doi.org/10.1016/j.jcou.2019.03.009).
- 58 O. H. Laguna, M. I. Domínguez, S. Oraá, A. Navajas, G. Arzamendi, L. M. Gandía, *et al.*, Influence of the O<sub>2</sub>/CO ratio and the presence of H<sub>2</sub>O and CO<sub>2</sub> in the feed-stream during the preferential oxidation of CO (PROX) over a CuOx/CeO<sub>2</sub>-coated microchannel reactor, *Catal. Today*, 2013, **203**, 182–187, DOI: [10.1016/j.cattod.2012.04.021](https://doi.org/10.1016/j.cattod.2012.04.021).
- 59 M. González-Castaño, T. R. Reina, S. Ivanova, L. M. Martínez Tejada, M. A. Centeno and J. A. Odriozola, O<sub>2</sub>-assisted Water Gas Shift reaction over structured Au and Pt catalysts, *Appl. Catal., B*, 2016, **185**, 337–343, DOI: [10.1016/j.apcatb.2015.12.032](https://doi.org/10.1016/j.apcatb.2015.12.032).
- 60 O. U. Valdés-Martínez, V. A. Suárez-Toriello, J. d. I. Reyes, B. Pawelec and J. L. G. Fierro, Support effect and metals interactions for NiRu/Al<sub>2</sub>O<sub>3</sub>, TiO<sub>2</sub> and ZrO<sub>2</sub> catalysts in the hydrodeoxygenation of phenol, *Catal. Today*, 2017, **296**, 219–227, DOI: [10.1016/j.cattod.2017.04.007](https://doi.org/10.1016/j.cattod.2017.04.007).
- 61 L. Pastor-Pérez, R. Buitrago-sierra and A. Sepulveda-Escribano, CeO<sub>2</sub>-promoted Ni/activated carbon catalysts for the water-gas shift (WGS) reaction, *Int. J. Hydrogen Energy*, 2014, **9**, 17589–17599, DOI: [10.1016/j.ijhydene.2014.08.089](https://doi.org/10.1016/j.ijhydene.2014.08.089).
- 62 L. Pastor-Pérez and A. Sepúlveda-Escribano, Multicomponent NiSnCeO<sub>2</sub>/C catalysts for the low-temperature glycerol steam reforming, *Appl. Catal., A*, 2017, **529**, 118–126, DOI: [10.1016/j.apcata.2016.10.022](https://doi.org/10.1016/j.apcata.2016.10.022).
- 63 S. C. Rood, H. B. Ahmet, A. Gomez-Ramon, L. Torrente-Murciano, T. R. Reina and S. Eslava, Enhanced ceria nanoflakes using graphene oxide as a sacrificial template for CO oxidation and dry reforming of methane, *Appl. Catal., B*, 2019, **242**, 358–368, DOI: [10.1016/j.apcatb.2018.10.011](https://doi.org/10.1016/j.apcatb.2018.10.011).
- 64 Q. Pan, J. Peng, T. Sun, S. Wang and S. Wang, Insight into the reaction route of CO<sub>2</sub> methanation: Promotion effect of medium basic sites, *Catal. Commun.*, 2014, **45**, 74–78, DOI: [10.1016/j.catcom.2013.10.034](https://doi.org/10.1016/j.catcom.2013.10.034).
- 65 P. Gruene, A. G. Belova, T. M. Yegulalp, R. J. Farrauto and M. J. Castaldi, Dispersed calcium oxide as a reversible and efficient CO<sub>2</sub>sorbent at intermediate temperatures, *Ind. Eng. Chem. Res.*, 2011, **50**, 4042–4049, DOI: [10.1021/ie102475d](https://doi.org/10.1021/ie102475d).
- 66 A. Ali Khan and M. Tahir, Construction of an S-Scheme Heterojunction with Oxygen-Vacancy-Rich Trimetallic CoAlLa-LDH Anchored on Titania-Sandwiched Ti<sub>3</sub>C<sub>2</sub>Multilayers for Boosting Photocatalytic CO<sub>2</sub>Reduction under Visible Light, *Ind. Eng. Chem. Res.*, 2021, **60**, 16201–16223, DOI: [10.1021/acs.iecr.1c03242](https://doi.org/10.1021/acs.iecr.1c03242).
- 67 B. Tahir, M. Tahir and N. A. S. Amin, Ag-La loaded protonated carbon nitrides nanotubes (pCNNT) with improved charge separation in a monolithic honeycomb photoreactor for enhanced bioreforming of methane (BRM) to fuels, *Appl. Catal., B*, 2019, **248**, 167–183, DOI: [10.1016/j.apcatb.2019.01.076](https://doi.org/10.1016/j.apcatb.2019.01.076).
- 68 J. M. Lavoie, Review on dry reforming of methane, a potentially more environmentally-friendly approach to the increasing natural gas exploitation, *Front. Chem.*, 2014, **2**, 1–17, DOI: [10.3389/fchem.2014.00081](https://doi.org/10.3389/fchem.2014.00081).
- 69 E. Le Saché, S. Johnson, L. Pastor-Pérez, B. A. Horri and T. R. Reina, Biogas upgrading via dry reforming over a Ni-Sn/CeO<sub>2</sub>-Al<sub>2</sub>O<sub>3</sub> catalyst: Influence of the biogas source, *Energies*, 2019, **12**(6), 1007, DOI: [10.3390/en12061007](https://doi.org/10.3390/en12061007).
- 70 K. Tao, L. Shi, Q. Ma, D. Wang, C. Zeng, C. Kong, *et al.*, Methane reforming with carbon dioxide over mesoporous nickel-alumina composite catalyst, *Chem. Eng. J.*, 2013, **221**, 25–31, DOI: [10.1016/j.cej.2013.01.073](https://doi.org/10.1016/j.cej.2013.01.073).
- 71 S. Wang, R. J. Farrauto, S. Karp, J. H. Jeon and E. T. Schruk, Parametric, cyclic aging and characterization studies for CO<sub>2</sub> capture from flue gas and catalytic conversion to synthetic natural gas using a dual functional material (DFM), *J. CO<sub>2</sub> Util.*, 2018, **27**, 390–397, DOI: [10.1016/j.jcou.2018.08.012](https://doi.org/10.1016/j.jcou.2018.08.012).
- 72 A. Bermejo-López, B. Pereda-Ayo, J. A. González-Marcos and J. R. González-Velasco, Mechanism of the CO<sub>2</sub> storage and in situ hydrogenation to CH<sub>4</sub>. Temperature and adsorbent loading effects over Ru-CaO/Al<sub>2</sub>O<sub>3</sub> and Ru-Na<sub>2</sub>CO<sub>3</sub>/Al<sub>2</sub>O<sub>3</sub> catalysts, *Appl. Catal., B*, 2019, **256**, 117845, DOI: [10.1016/j.apcatb.2019.117845](https://doi.org/10.1016/j.apcatb.2019.117845).
- 73 T. Stroud, T. J. Smith, E. Le Saché, J. L. Santos, M. A. Centeno, H. Arellano-Garcia, *et al.*, Chemical CO<sub>2</sub> recycling via dry and bi reforming of methane using Ni-Sn/Al<sub>2</sub>O<sub>3</sub> and Ni-Sn/CeO<sub>2</sub>-Al<sub>2</sub>O<sub>3</sub> catalysts, *Appl. Catal., B*, 2018, **224**, 125–135, DOI: [10.1016/j.apcatb.2017.10.047](https://doi.org/10.1016/j.apcatb.2017.10.047).
- 74 D. Kutyła, K. Kołczyk-Siedlecka, A. Kwiecińska, K. Skibińska, R. Kowalik and P. Żabiński, Preparation and characterization of electrodeposited Ni-Ru alloys : morphological and catalytic study, *J. Solid State Electrochem.*, 2019, **23**, 3089–3097, DOI: [10.1007/s10008-019-04374-7](https://doi.org/10.1007/s10008-019-04374-7).
- 75 Q. Zheng, R. Farrauto and A. Chau Nguyen, Adsorption and Methanation of Flue Gas CO<sub>2</sub> with Dual Functional Catalytic Materials: A Parametric Study, *Ind. Eng. Chem. Res.*, 2016, **55**, 6768–6776, DOI: [10.1021/acs.iecr.6b01275](https://doi.org/10.1021/acs.iecr.6b01275).
- 76 S. Cimino, E. M. Cepollaro and L. Lisi, Sulfur tolerance and self-regeneration mechanism of Na-Ru/Al<sub>2</sub>O<sub>3</sub> dual function material during the cyclic CO<sub>2</sub> capture and catalytic methanation, *Appl. Catal., B*, 2022, **317**, 121705, DOI: [10.1016/j.apcatb.2022.121705](https://doi.org/10.1016/j.apcatb.2022.121705).

